

One-loop expressions for $h \rightarrow l\bar{l}\gamma$ in Higgs extensions of the Standard Model

L. T. Hue^{a,b}, Dzung Tri Tran^{c,d}, Thanh Huy Nguyen^e, Khiem Hong Phan^{c,d}

^a *Subatomic Physics Research Group, Science and Technology Advanced Institute, Van Lang University, Ho Chi Minh City 70000, Vietnam*

^b *Faculty of Applied Technology, School of Technology, Van Lang University, Ho Chi Minh City 70000, Vietnam*

^c *Institute of Fundamental and Applied Sciences, Duy Tan University, Ho Chi Minh City 700000, Vietnam*

^d *Faculty of Natural Sciences, Duy Tan University, Da Nang City 550000, Vietnam*

^e *University of Science Ho Chi Minh City, 227 Nguyen Van Cu, District 5, Ho Chi Minh City, Vietnam*

Abstract

A systematic study of one-loop contributions to the decay channels $h \rightarrow l\bar{l}\gamma$ with $l = \nu_{e,\mu,\tau}, e, \mu$, performed in Higgs extended versions of the Standard Model, is presented in the 't Hooft-Veltman gauge. Analytic formulas for one-loop form factors are expressed in terms of the logarithm and di-logarithmic functions. As a result, these form factors can be reduced to those relating to the loop-induced decay processes $h \rightarrow \gamma\gamma, Z\gamma$, confirming not only previous results using different approaches but also close relations between the three kinds of the loop-induced Higgs decay rates. For phenomenological study, we focus on the two observables, namely the enhancement factors defined as ratios of the decay rates calculated between the Higgs extended versions and the standard model, and the forward-backward asymmetries of fermions, which can be used to search for Higgs extensions of the SM. We show that direct effects of mixing between neutral Higgs bosons and indirect contributions of charged Higgs boson exchanges can be probed at future colliders.

Keywords: *Higgs phenomenology, Physics beyond the Standard Models, One-loop Feynman integrals, Analytic methods for Quantum Field Theory, Dimensional regularization, Future colliders.*

1. Introduction

Future colliders such as the High-Luminosity Large Hadron Collider (HL-LHC) [1, 2] and International Linear Collider (LC) [3] focus greatly on the precise measurements for the properties of the Standard Model-like (SM-like) Higgs boson. The measurements provide an important information to answer the nature of the electroweak spontaneous symmetry breaking (EWSB)—in other words, to verify the structure of scalar potential. It is well-known that the Higgs potential of the SM is the simplest such that a scalar doublet is only taken into account for EWSB. In some Higgs extended version of the SM (called as HESM hereafter), the respective scalar potential is enlarged by including new scalar particles such as neutral, singly and doubly charged Higgs bosons, etc. They could contribute the decay channels of the SM-like Higgs boson and these effects could be tested at future colliders. Recently, the loop-induced decays of the SM-like Higgs boson (h) into $\gamma\gamma$ [4, 5] and $Z\gamma$ have been probed at the LHC [6, 7, 8, 9]. Together with $h \rightarrow Z\gamma, \gamma\gamma$, the decay processes $h \rightarrow f\bar{f}\gamma$ with $l = \nu_{e,\mu,\tau}, e, \mu$ also play a key role for testing the SM [14, 15, 16] and constraining parameters of many models beyond the SM (BSMs) [16].

Email addresses: lethohue@vlu.edu.vn (L. T. Hue), phan hong khiem@duytan.edu.vn (Khiem Hong Phan)

More recently, the decay channels $h \rightarrow f\bar{f}\gamma$ have been greatly paid attention at the LHC [10, 11, 12, 13].

From the theoretical viewpoint, one-loop corrections to $h \rightarrow f\bar{f}\gamma$ are important for matching high-precision data at future colliders. In the SM, many calculations for these one-loop corrections were reported in Refs. [17, 18, 19, 20, 21, 22, 23, 24]. One-loop formulas for $h \rightarrow f\bar{f}\gamma$ in Two Higgs Doublet Models (THDM) were computed in Refs. [25, 26]. In our previous works [27, 28], we have performed the evaluations for one-loop contributions to $h \rightarrow l\bar{l}\gamma$ in general BSM frameworks. The computations have done in the unitarity gauge. It is well-known that the results for one-loop contributions to $h \rightarrow \gamma\gamma, Z\gamma$ in unitarity gauge may face to large numerical cancellations [29, 32], because the higher-rank tensor one-loop integrals appear from Feynman diagrams containing gauge boson exchanges in the loops. The same problem may occur in the computations for one-loop contributions to the decays $h \rightarrow l\bar{l}\gamma$. In particular, the issue may appear in boundary of the phase space in which low-values of the invariant mass of lepton-pair, lepton-photon and the low-energy of photon is applied, and the case that the photon may go nearly parallel to the lepton momenta. To cure these problems, several solutions are proposed such as evaluating the decay processes in the general space-time with dimension d [27, 28, 32], or considering the calculations in the 't Hooft-Feynman (HF) gauge [33].

Motivation from the above issues and confirming the consistent results in different gauges – checking the gauge invariance of the results, gaining the stability of the numerical results in full kinematic regions of the mentioned decay channels, we study systematically one-loop corrections to the decay channels $h \rightarrow l\bar{l}\gamma$ with $l = \nu_{e,\mu,\tau}, e, \mu$ in the HF gauge. In the limit of this paper, we consider the decay processes $h \rightarrow l\bar{l}\gamma$ with $l = \nu_{e,\mu,\tau}, e, \mu$ within HESM. In further detail, one-loop analytical formulas for the form factors are written in terms of scalar one-loop integrals which are then expressed with reference to the logarithm and di-logarithmic functions. One-loop form factors in this work can be also reduced to the corresponding ones for the decay channels $h \rightarrow \gamma\gamma, Z\gamma$ and these results confirm the previous results which are available in the SM as well as HESM. In phenomenological results, we show the enhancement factor in the Higgs extension for the SM models. Last but not least, the forward-backward (FB) asymmetries of fermions are also studied in this paper. Other beyond the SM frameworks such as the left-right models (LR) constructed from the $SU(2)_L \times SU(2)_R \times U(1)_Y$ [34, 35, 36], the 3-3-1 models ($SU(3)_L \times U(1)_X$) [37, 38, 39, 40, 41, 42, 43], the 3-4-1 models ($SU(4)_L \times U(1)_X$) [43, 44, 45, 46, 47, 48], etc, will be addressed in our future works.

The layout of our work is as follows. In section 2, we review three specific HESMs investigated in detail in our work, namely the Inert Doublet (IDM), THDM, and Triplet-Higgs (THM) models. Section 3 shows the detailed evaluations for one-loop contributions to the decay amplitudes $h \rightarrow l\bar{l}\gamma$. Phenomenological results for all mentioned HESMs are analyzed in section 4. Conclusions and outlook are devoted in section 5. Four appendices show more detailed expressions of the relevant couplings used in our calculations, precise expressions of scalar one-loop integrals in terms of di-logarithm functions, the finite and consistent results of the form factors being independent with the ultraviolet divergent part $1/\epsilon$ and the renormalization scale μ^2 , and the basis integrals relating to previous calculations.

2. Higgs extended versions of the Standard Model

This section will review specific models corresponding to the HESMs we are interested in this work. The simplest case is the SM extension adding a singlet neutral Higgs boson. As a result, the respective analytical expressions for the decay rates $h \rightarrow l\bar{l}\gamma$ are the same as those predicted by the SM, except an overall factor relating to the mixing angle between neutral Higgs bosons. For this reason, we will pay attention to the more interesting models, namely the IDM,

THDM, and the real Triplet Higgs Model (THM), which consist of charged Higgs bosons giving new one-loop contributions to the decay amplitudes under consideration.

2.1. The IDM

The IDM is constructed by adding into the SM an inert scalar $SU(2)_L$ doublet, which provide stable particles playing roles as dark matter candidates [49, 50, 51, 52, 53, 54, 55, 56, 57, 58, 59, 60, 61]. The Higgs potential corresponding to the renormalizable and gauge invariant theory is:

$$\begin{aligned} \mathcal{V}(\Phi_1, \Phi_2) = & \mu_1^2 |\Phi_1|^2 + \mu_2^2 |\Phi_2|^2 + \lambda_1 |\Phi_1|^4 + \lambda_2 |\Phi_2|^4 + \lambda_3 |\Phi_1|^2 |\Phi_2|^2 \\ & + \lambda_4 |\Phi_1^\dagger \Phi_2|^2 + \frac{\lambda_5}{2} \left\{ (\Phi_1^\dagger \Phi_2)^2 + \text{h.c.} \right\}, \end{aligned} \quad (1)$$

where an additional unbroken global Z_2 -symmetry is imposed, namely $\Phi_1 \leftrightarrow -\Phi_1$ is odd, while $\Phi_2 \leftrightarrow \Phi_2$ and all SM particles are even. Because Z_2 is maintained after the EWSB, all Φ_2 components develop the zero of vacuum expectation values (VEV), leading to the following expansions around VEV of the Higgs components:

$$\Phi_1 = \begin{pmatrix} G^\pm \\ \frac{1}{\sqrt{2}}(v + h + iG^0) \end{pmatrix}, \quad \Phi_2 = \begin{pmatrix} H^\pm \\ \frac{1}{\sqrt{2}}(H + iA^0) \end{pmatrix}, \quad (2)$$

where G^0 , G^\pm are Nambu-Goldstone bosons absorbed by the massive gauge bosons Z and W^\pm , respectively. In addition, there is no mixing of the two neutral components h and H . After EWSB, the matching condition with the SM results in $v = 246$ GeV as the electroweak scale. The IDM consist of three neutral physical states, in which h is identified as the SM-like Higgs boson observed at the LHC, while H and A^0 are the two CP-even and -odd ones predicted by the IDM. This model also predicts a pair of singly charged Higgs bosons H^\pm . All Higgs boson masses are functions of the parameters $\mu_1, \mu_2, \lambda_1, \dots, \lambda_5$, namely:

$$m_h^2 = -2\mu_1^2 = 2\lambda_1 v^2, \quad (3)$$

$$M_H^2 = \mu_2^2 + \frac{v^2}{2} (\lambda_3 + \lambda_4 + \lambda_5), \quad (4)$$

$$M_{A^0}^2 = \mu_2^2 + \frac{v^2}{2} (\lambda_3 + \lambda_4 - \lambda_5), \quad (5)$$

$$M_{H^\pm}^2 = \mu_2^2 + \frac{v^2}{2} \lambda_3. \quad (6)$$

Due to the unbroken Z_2 -symmetry, all "inert" Higgs bosons H, A^0 and H^\pm are odd under Z_2 , therefore they do not interact with quarks and leptons. As the result, the lightest neutral Higgs boson (H or A^0) is a dark matter candidate. The set of scanning parameters chosen in our analysis is

$$\mathcal{P}_{\text{IDM}} = \{\mu_2^2, \lambda_2^2, m_h^2, M_H^2, M_{A^0}^2, M_{H^\pm}^2\}. \quad (7)$$

The Yukawa Lagrangian of this model is exactly the same as that of the SM, namely

$$\mathcal{L}_{\text{Yukawa}} = - \sum_{f=u,d,l} g_{hff}^{\text{IDM}} h \bar{f} f + \dots, \quad (8)$$

where $g_{hff}^{\text{IDM}} = g_{hff}^{\text{SM}} = m_f/v$, and f is a SM lepton with mass m_f . All related couplings to the decay channels $h \rightarrow \ell \bar{\ell} \gamma$ are listed in Table 1, see a detailed derivation in Appendix A.

Vertices	Notations	Couplings
$hH^\pm H^\mp$	$g_{hH^\pm H^\mp}^{\text{IDM}}$	$-i \frac{2(M_{H^\pm}^2 - \mu_2^2)}{v}$
$Z_\mu H^\pm(p^+) H^\mp(p^-)$	$g_{ZH^\pm H^\mp}^{\text{IDM}}$	$\frac{M_Z}{v} c_{2W} (p^+ - p^-)_\mu$
$A_\mu H^\pm(p^+) H^\mp(p^-)$	$g_{AH^\pm H^\mp}^{\text{IDM}}$	$\frac{M_Z}{v} s_{2W} (p^+ - p^-)_\mu$
$h f \bar{f}$	$g_{h f \bar{f}}^{\text{IDM}}$	$i m_f / v$

Table 1: All couplings giving one-loop contribution to the decay amplitudes $H \rightarrow l\bar{l}\gamma$ in the IDM. Here A_μ is the photon field, p^\pm is the incoming momentum of H^\pm , $s_W(c_W)$ is sine (and cosine) of the Weinberg's angle, respectively.

2.2. THDM

The second HESM considered in this work is the THDM, in which a new complex Higgs doublet with the hypercharge $Y = 1/2$ is added into the SM, see Ref.[62] for a detailed theoretical and phenomenological review. The renormalizable and gauge invariant Higgs potential is

$$\begin{aligned} \mathcal{V}(\Phi_1, \Phi_2) = & m_{11}^2 \Phi_1^\dagger \Phi_1 + m_{22}^2 \Phi_2^\dagger \Phi_2 - [m_{12}^2 \Phi_1^\dagger \Phi_2 + \text{h.c.}] + \frac{\lambda_1}{2} (\Phi_1^\dagger \Phi_1)^2 + \frac{\lambda_2}{2} (\Phi_2^\dagger \Phi_2)^2 \\ & + \lambda_3 (\Phi_1^\dagger \Phi_1) (\Phi_2^\dagger \Phi_2) + \lambda_4 (\Phi_1^\dagger \Phi_2) (\Phi_2^\dagger \Phi_1) + \frac{1}{2} [\lambda_5 (\Phi_1^\dagger \Phi_2)^2 + \text{h.c.}]. \end{aligned} \quad (9)$$

For the EWSB, two scalar doublets can be written as

$$\Phi_1 = \begin{bmatrix} \phi_1^+ \\ (v_1 + \rho_1 + i\eta_1)/\sqrt{2} \end{bmatrix} \quad \text{and} \quad \Phi_2 = \begin{bmatrix} \phi_2^+ \\ (v_2 + \rho_2 + i\eta_2)/\sqrt{2} \end{bmatrix}, \quad (10)$$

where $v = \sqrt{v_1^2 + v_2^2} = 246$ GeV from the matching condition with the SM. After EWSB, the THDM consist of two CP-even Higgs bosons h and H , a CP-odd A^0 , and a pair of singly charged ones H^\pm . One of them, namely h is identified with the SM-like Higgs boson discovered at LHC.

The mass and flavor base of all Higgs bosons relate to each other by the following rotations

$$\begin{pmatrix} \phi_1^\pm \\ \phi_2^\pm \end{pmatrix} = \begin{pmatrix} c_\beta & -s_\beta \\ s_\beta & c_\beta \end{pmatrix} \begin{pmatrix} G^\pm \\ H^\pm \end{pmatrix}, \quad (11)$$

$$\begin{pmatrix} \rho_1 \\ \rho_2 \end{pmatrix} = \begin{pmatrix} c_\alpha & -s_\alpha \\ s_\alpha & c_\alpha \end{pmatrix} \begin{pmatrix} h \\ H \end{pmatrix}, \quad (12)$$

and

$$\begin{pmatrix} \eta_1 \\ \eta_2 \end{pmatrix} = \begin{pmatrix} c_\beta & -s_\beta \\ s_\beta & c_\beta \end{pmatrix} \begin{pmatrix} G^0 \\ A^0 \end{pmatrix}. \quad (13)$$

where the mixing α between two neutral Higgs is taken into account and β is the mixing angle defined as $t_\beta \equiv \tan \beta = v_2/v_1$. All Higgs boson masses are determined as follows:

$$M_{H^\pm}^2 = \mu^2 - \frac{1}{2}(\lambda_4 + \lambda_5)v^2, \quad (14)$$

$$M_{A^0}^2 = \mu^2 - \lambda_5 v^2, \quad (15)$$

$$m_h^2 = M_{11}^2 s_{\beta-\alpha}^2 + M_{22}^2 c_{\beta-\alpha}^2 + M_{12}^2 s_{2(\beta-\alpha)}, \quad (16)$$

$$M_H^2 = M_{11}^2 c_{\beta-\alpha}^2 + M_{22}^2 s_{\beta-\alpha}^2 - M_{12}^2 s_{2(\beta-\alpha)}, \quad (17)$$

where $\mu^2 = m_{12}^2/(s_\beta c_\beta)$, $s_{2x} \equiv 2s_x c_x$, $c_{2x} \equiv c_x^2 - s_x^2$ ($x = \beta - \alpha, \beta$),

$$M_{11}^2 = (\lambda_1 c_\beta^4 + \lambda_2 s_\beta^4) v^2 + \frac{v^2}{2} (\lambda_3 + \lambda_4 + \lambda_5) s_{2\beta}^2, \quad (18)$$

$$M_{22}^2 = \mu^2 + \frac{v^2}{4} [\lambda_1 + \lambda_2 - 2(\lambda_3 + \lambda_4 + \lambda_5)] s_{2\beta}^2, \quad (19)$$

$$M_{12}^2 = -\frac{v^2}{2} [\lambda_1 c_\beta^2 - \lambda_2 s_\beta^2 - (\lambda_3 + \lambda_4 + \lambda_5) c_{2\beta}] s_{2\beta}. \quad (20)$$

All couplings involving the decay processes under consideration were presented in detail in [Appendix A](#), where the couplings between Higgs and gauge bosons are listed in [Table 2](#).

Vertices	Notations	Couplings
$hW_\mu W_\nu$	g_{hWW}^{THDM}	$-i \frac{2M_W^2}{v} s_{\beta-\alpha} g_{\mu\nu}$
$hZ_\mu Z_\nu$	g_{hZZ}^{THDM}	$-i \frac{2M_Z^2}{v} s_{\beta-\alpha} g_{\mu\nu}$
$hH^\pm H^\mp$	$g_{hH^\pm H^\mp}^{\text{THDM}}$	$-\frac{i}{v} [(2\mu^2 - 2M_{H^\pm}^2 - m_h^2) s_{\beta-\alpha} + 2 \cot(2\beta) (\mu^2 - m_h^2) c_{\beta-\alpha}]$
$Z_\mu H^\pm(p^+) H^\mp(p^-)$	$g_{ZH^\pm H^\mp}^{\text{THDM}}$	$\frac{M_Z}{v} c_{2W} (p^+ - p^-)_\mu$
$A_\mu H^\pm(p^+) H^\mp(p^-)$	$g_{AH^\pm H^\mp}^{\text{THDM}}$	$\frac{M_Z}{v} s_{2W} (p^+ - p^-)_\mu$

Table 2: All the couplings involving the decay processes $h \rightarrow l\bar{l}\gamma$ in the THDM. A_μ is photon field.

The Yukawa Lagrangian written in terms of the mass eigenstates is [\[62\]](#)

$$\mathcal{L}_{\text{Yukawa}} = - \sum_{f=u,d,l} (g_{hff}^{\text{THDM}} \bar{f} f h + g_{Hff}^{\text{THDM}} \bar{f} f H - i g_{A^0 ff}^{\text{THDM}} \bar{f} \gamma_5 f A^0) + \dots, \quad (21)$$

where particular formulas for different types of the THDM were shown in [Appendix A](#), see the final results presented in [Table 3](#). In the limit of $s_{\beta-\alpha} \rightarrow 1$, called as h^{SM} -scenario, one has

$$g_{hH^\pm H^\mp}^{\text{THDM}} \rightarrow -i \frac{(2\mu^2 - 2M_{H^\pm}^2 - m_h^2)}{v} s_{\beta-\alpha}. \quad (22)$$

In the case of THDM, Finally, the set $\mathcal{P}_{\text{THDM}}$ of scanning parameters used for our numerical investigation is chosen as follows

$$\mathcal{P}_{\text{THDM}} = \{m_h^2, M_H^2, M_{A^0}^2, M_{H^\pm}^2, m_{12}^2, t_\beta, s_{\beta-\alpha}\}. \quad (23)$$

Type	$g_{h_uu}^{\text{THDM}}$	$g_{h_{dd}}^{\text{THDM}}$	$g_{h_{ll}}^{\text{THDM}}$
I	$\frac{m_u}{\sqrt{2}v} \frac{c_\alpha}{s_\beta}$	$\frac{m_d}{\sqrt{2}v} \frac{c_\alpha}{s_\beta}$	$\frac{m_l}{\sqrt{2}v} \frac{c_\alpha}{s_\beta}$
II	$\frac{m_u}{\sqrt{2}v} \frac{c_\alpha}{s_\beta}$	$-\frac{m_d}{\sqrt{2}v} \frac{s_\alpha}{c_\beta}$	$-\frac{m_l}{\sqrt{2}v} \frac{s_\alpha}{c_\beta}$
X	$\frac{m_u}{\sqrt{2}v} \frac{c_\alpha}{s_\beta}$	$\frac{m_d}{\sqrt{2}v} \frac{c_\alpha}{s_\beta}$	$-\frac{m_l}{\sqrt{2}v} \frac{s_\alpha}{c_\beta}$
Y	$\frac{m_u}{\sqrt{2}v} \frac{c_\alpha}{s_\beta}$	$-\frac{m_d}{\sqrt{2}v} \frac{s_\alpha}{c_\beta}$	$\frac{m_l}{\sqrt{2}v} \frac{c_\alpha}{s_\beta}$

Table 3: The Yukawa couplings in THDMs with type I,II, X, and Y respectively.

2.3. THM

We finally mention THM, which is the SM adding only one additional real Higgs triplet, denoted as Δ with $Y_\Delta = 2$ [71, 72, 73, 74, 75, 76, 77, 78, 79, 80, 81, 82, 84, 85, 86]. The renormalizable gauge invariant Higgs potential is

$$\begin{aligned} \mathcal{V}(\Phi, \Delta) = & -m_\Phi^2 \Phi^\dagger \Phi + \frac{\lambda}{4} (\Phi^\dagger \Phi)^2 + M_\Delta^2 \text{Tr}(\Delta^\dagger \Delta) + [\mu (\Phi^T i \sigma^2 \Delta^\dagger \Phi) + \text{h.c.}] \\ & + \lambda_1 (\Phi^\dagger \Phi) \text{Tr}(\Delta^\dagger \Delta) + \lambda_2 (\text{Tr} \Delta^\dagger \Delta)^2 + \lambda_3 \text{Tr}(\Delta^\dagger \Delta)^2 + \lambda_4 \Phi^\dagger \Delta \Delta^\dagger \Phi, \end{aligned} \quad (24)$$

where σ^2 is Pauli matrix, and all Higgs self couplings λ_i ($i = \overline{1,4}$) are real. For the EWSB, two Higgs multiplets are parameterized as follows:

$$\Delta = \begin{bmatrix} \frac{\delta^+}{\sqrt{2}} & \delta^{++} \\ \frac{1}{\sqrt{2}}(v_\Delta + \eta_\Delta + i\chi_\Delta) & -\frac{\delta^+}{\sqrt{2}} \end{bmatrix} \quad \text{and} \quad \Phi = \begin{bmatrix} \phi^+ \\ \frac{1}{\sqrt{2}}(v_\Phi + \eta_\Phi + i\chi_\Phi) \end{bmatrix}, \quad (25)$$

where v_Φ and v_Δ are correspondingly the VEVs of the two neutral Higgs components. The electroweak scale is $v = \sqrt{v_\Phi^2 + 2v_\Delta^2} = 246$ GeV when matching with the SM.

After EWSB, the physical Higgs spectrum of the THM consist of two pairs of charged Higgs bosons, namely doubly $H^{\pm\pm}$ and singly H^\pm , a neutral CP-odd A^0 , and two CP-even H and h being identified with the SM-like Higgs boson. The relations between two mass and flavor base are

$$\begin{pmatrix} \phi^\pm \\ \delta^\pm \end{pmatrix} = \begin{pmatrix} c_{\beta^\pm} & -s_{\beta^\pm} \\ s_{\beta^\pm} & c_{\beta^\pm} \end{pmatrix} \begin{pmatrix} G^\pm \\ H^\pm \end{pmatrix}, \quad (26)$$

$$\begin{pmatrix} \eta_\Phi \\ \eta_\Delta \end{pmatrix} = \begin{pmatrix} c_\alpha & -s_\alpha \\ s_\alpha & c_\alpha \end{pmatrix} \begin{pmatrix} h \\ H \end{pmatrix}, \quad (27)$$

and

$$\begin{pmatrix} \chi_\Phi \\ \chi_\Delta \end{pmatrix} = \begin{pmatrix} c_{\beta^0} & -s_{\beta^0} \\ s_{\beta^0} & c_{\beta^0} \end{pmatrix} \begin{pmatrix} G^0 \\ A^0 \end{pmatrix}, \quad (28)$$

where $t_{\beta^\pm} = \frac{\sqrt{2}v_\Delta}{v_\Phi}$, $t_{\beta^0} = \sqrt{2}t_{\beta^\pm}$ and the mixing angles α between two neutral Higgs is taken into account. Their masses are functions of Higgs self couplings and μ as follows

$$M_{H^{\pm\pm}}^2 = \frac{\sqrt{2}\mu v_\Phi^2 - \lambda_4 v_\Phi^2 v_\Delta - 2\lambda_3 v_\Delta^3}{2v_\Delta}, \quad (29)$$

$$M_{H^\pm}^2 = \frac{(v_\Phi^2 + 2v_\Delta^2) [2\sqrt{2}\mu - \lambda_4 v_\Delta]}{4v_\Delta}, \quad (30)$$

$$M_{A^0}^2 = \frac{\mu(v_\Phi^2 + 4v_\Delta^2)}{\sqrt{2}v_\Delta}, \quad (31)$$

$$M_H^2 = \frac{1}{2} \left\{ \lambda v_\Phi^2 s_\alpha^2 + c_\alpha^2 \left[\sqrt{2}\mu \frac{v_\Phi^2}{v_\Delta} \left(1 + 4\frac{v_\Delta}{v_\Phi} t_\alpha \right) + 4v_\Delta^2 \left((\lambda_2 + \lambda_3) - (\lambda_1 + \lambda_4) \frac{v_\Phi}{v_\Delta} t_\alpha \right) \right] \right\}, \quad (32)$$

$$m_h^2 = \frac{1}{2} \left\{ \lambda v_\Phi^2 c_\alpha^2 + s_\alpha^2 \left[\sqrt{2}\mu \frac{v_\Phi^2}{v_\Delta} \left(1 - 4\frac{v_\Delta}{v_\Phi} t_\alpha \right) + 4v_\Delta^2 \left((\lambda_1 + \lambda_4) \frac{v_\Phi}{v_\Delta} t_\alpha + (\lambda_2 + \lambda_3) \right) \right] \right\}. \quad (33)$$

The Yukawa Lagrangian is written in terms of the mass eigenstates as follows

$$\mathcal{L}_{\text{Yukawa}} = \mathcal{L}_{\text{Yukawa}}^{\text{SM}} - L^T y_\nu C(i\sigma^2 \Delta) L + \text{h.c.}, \quad (34)$$

where $L = (L_e, L_\mu, L_\tau)$ consists of three left-handed lepton doublets, y_ν is the 3×3 Yukawa coupling matrix generating the neutrino masses, and C is the charge conjugation operator. Expanding the Yukawa Lagrangian and the Higgs potential in the mass basis of all particles, we derived all couplings that give one-loop contributions to the decay amplitudes $h \rightarrow f \bar{f} \gamma$. The respective vertices are presented in Table 4, see a detailed derivation given in Appendix A.

It is noted that in the limit of $\frac{v_\Delta}{v} \rightarrow 0$, we have

$$\frac{s_\alpha}{v_\Delta} \simeq \frac{v}{(m_h^2 - M_{A^0}^2)c_\alpha} \left(\lambda_1 + \frac{2M_{A^0}^2 - 4M_{H^\pm}^2}{v^2} \right) + \mathcal{O}\left(\frac{v_\Delta^2}{v^2}\right). \quad (35)$$

All above couplings can be obtained appropriately by using the relation in (35) in this limit.

In the THM, all parameters used in our analysis are

$$\mathcal{P}_{\text{THM}} = \{m_h^2, M_H^2, M_{A^0}^2, M_{H^\pm}^2, M_{H^{\pm\pm}}^2, t_{\beta^\pm}, s_\alpha\}. \quad (36)$$

3. One-loop expressions for $h \rightarrow l \bar{l} \gamma$ in HESMs

In order to generalize one-loop expressions for $h \rightarrow l(q_1) \bar{l}(q_2) \gamma(q_3)$ in the HESMs considered in this work, we define the following notations. The common notation $g_{\text{vertex}}^{(\text{NP})}$ denotes all vertices appearing in the HESMs with NP \equiv IDM, THDM and THM. These couplings were listed in Tables 1, 2, 3, and 4 for particular HESM. Noting that we use f for all internal fermions exchanging in the loop and l is for external fermions in our computations. For this calculation, we choose to work in the on-shell renormalization scheme, hence no diagrams giving one-loop corrections to external legs. In the HF gauge, all one-loop Feynman diagrams can be separated into two following groups. Group 1 includes all V^* -pole diagrams $h \rightarrow V^* \gamma \rightarrow l \bar{l} \gamma$, where the V^* exchange may be neutral or charged gauge Z^*, γ^* , or Higgs S^* bosons, as described in Figs. 1, 2, and 3, where particle exchange in loops may be fermions, gauge bosons, Nambu-Goldstone, Higgs bosons or Ghost particles. A V^* -pole diagram is realized as it always consists of a virtual boson V^* decaying into two final lepton states through the vertex $V^* \bar{l} l$. It is well-known that the sum of all diagrams given in Fig. 2 vanishes for the final on-shell external photon [28]. Furthermore, we are going to collect only form factors relating with the parts proportional to $q^\mu q_3^\nu$ appearing in Eqs. (37, 55). Therefore, all diagrams in Fig. 3 are ignored in this work, because their contributions are always proportional to $g^{\mu\nu}$. Group 2 consists of all remaining Feynman diagrams giving none V^* -pole contributions to the decay amplitudes $h \rightarrow l \bar{l} \gamma$ (Non-pole contributions hereafter). This group contains several one-loop box diagrams, as given in Fig. 4.

Our calculations are performed as follows. We firstly make a model file in FeynArt [88], then use FormCalc [89] and FeynCalc [90] to generate automatically one-loop amplitudes. Related

Vertices	Notations	Couplings
$hW_\mu W_\nu$	g_{hWW}^{THM}	$-i\frac{2M_W^2}{v}(c_\alpha c_{\beta^\pm} + \sqrt{2}s_\alpha s_{\beta^\pm})g_{\mu\nu}$
$hZ_\mu Z_\nu$	g_{hZZ}^{THM}	$-i\frac{2M_Z^2}{\sqrt{v^2+2v_\Delta^2}}(c_{\beta^0}c_\alpha + 2s_{\beta^0}s_\alpha)g_{\mu\nu}$
$hH^\pm H^\mp$	$g_{hH^\pm H^\mp}^{\text{THM}}$	$-i\frac{c_\alpha}{v_\Phi}\left[2M_{H^\pm}^2\frac{v_\Phi^2}{v^2} + 2m_h^2\frac{v_\Delta^2}{v^2}\right]$ $-i\frac{s_\alpha}{v_\Delta}\left[4M_{H^\pm}^2\frac{v_\Delta^2}{v^2} + m_h^2\frac{v_\Phi^2}{v^2} - M_{A^0}^2\frac{v^2}{v^2+2v_\Delta^2}\right]$
$hH^{\pm\pm} H^{\mp\mp}$	$g_{hH^{\pm\pm} H^{\mp\mp}}^{\text{THM}}$	$-i\frac{2v_\Phi c_\alpha}{v_\Phi^2 + 4v_\Delta^2}\left[2M_{H^\pm}^2\left(1 + \frac{2v_\Delta^2}{v^2}\right) - M_{A^0}^2\right]$ $-i\frac{s_\alpha}{v_\Delta}\left[2M_{H^{\pm\pm}}^2 - 4M_{H^\pm}^2\frac{v_\Phi^2}{v^2} + m_h^2\right]$ $+M_{A^0}^2\left(1 - \frac{4v_\Delta^2}{v^2+2v_\Delta^2}\right)]$
$Z_\mu H^\pm H^\mp$	$g_{ZH^\pm H^\mp}^{\text{THM}}$	$\frac{M_Z}{\sqrt{v^2+2v_\Delta^2}}(c_W^2 - s_W^2 - c_{\beta^\pm}^2)(p^+ - p^-)_\mu$
$Z_\mu H^{\pm\pm} H^{\mp\mp}$	$g_{ZH^{\pm\pm} H^{\mp\mp}}^{\text{THM}}$	$\frac{2M_Z}{\sqrt{v^2+2v_\Delta^2}}(c_W^2 - s_W^2)(p^{++} - p^{--})_\mu$
$A_\mu H^\pm H^\mp$	$g_{AH^\pm H^\mp}^{\text{THM}}$	$e(p^+ - p^-)_\mu$
$A_\mu H^{\pm\pm} H^{\mp\mp}$	$g_{AH^{\pm\pm} H^{\mp\mp}}^{\text{THM}}$	$(2e)(p^{++} - p^{--})_\mu$
$hf\bar{f}$	$g_{hf\bar{f}}^{\text{THM}}$	$i\frac{m_f c_\alpha}{v c_{\beta^\pm}}$
$h\nu_l\bar{\nu}_l$	$g_{h\nu_l\bar{\nu}_l}^{\text{THM}}$	$i\frac{m_{\nu_l}}{v_\Delta}s_\alpha$

Table 4: The couplings involving the decay processes $h \rightarrow l\bar{l}\gamma$ in the THM. A_μ is the photon.

one-loop form factors are collected in terms of Passarino-Veltman (PV-) functions before transformed in terms of scalar one-loop integrals [89, 92]. We finally use `Package-X` [91] to perform the ϵ -expansions for scalar one-loop integrals with respect to logarithmic and di-logarithm functions.

3.1. V^* -pole contributions

As mentioned in the above arguments, it is enough to consider the contributions from diagrams given in Fig. 1. In principle, V^* -pole diagrams may appear with all $V^* = Z^*, \gamma^*$, and neutral Higgs bosons. Since the couplings of S^* to leptons are proportional to m_l/v in most of the HESMs, the later cases give much smaller contributions than the former ones. As a result, we only concern Z^*, γ^* -poles in the current work. Now, the one-loop amplitude can be decomposed

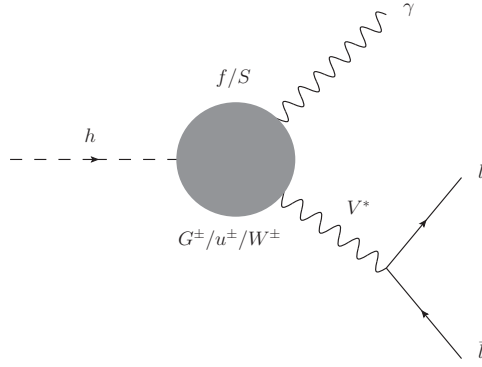


Figure 1: One-loop Feynman diagrams for the decay $h \rightarrow \bar{l}l\gamma$ belonging to group 1. Here S , G^\pm , and u^\pm are Higgs boson, Nambu-Goldstone bosons, and Ghost, respectively.

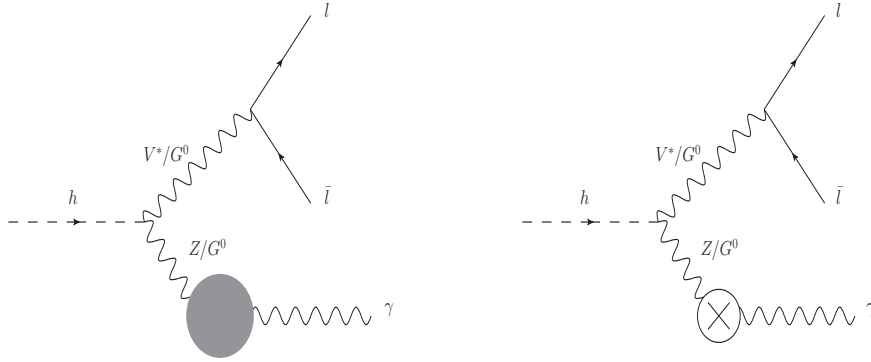


Figure 2: One-loop Feynman diagrams for the decay $h \rightarrow \bar{l}l\gamma$ in group 1. G^0 is the Nambu-Goldstone boson.

into the following Lorentz structures:

$$\mathcal{A}_{V^*\text{-pole}} = \sum_{V^*=\{\gamma^*, Z^*\}} F_{\gamma V^*}^{V^*\text{-pole}} \left[q^\mu q_3^\nu - (q \cdot q_3) g^{\mu\nu} \right] \left[\bar{u}(q_1) \gamma_\nu \left(\sum_{j=\{L,R\}} g_{V^* \bar{l} l}^j P_j \right) v(q_2) \right] \varepsilon_\mu^*(q_3), \quad (37)$$

where $q = q_1 + q_2$, $\varepsilon_\mu^*(q_3)$ is the final photon polarization, and

$$g_{V^* \bar{l} l}^j = \begin{cases} -eQ_l & \text{if } V^* \equiv \gamma^*, \\ \frac{e}{s_W c_W} \left(I_{3,l}^j - Q_l s_W^2 \right) & \text{if } V^* \equiv Z^* \end{cases} \quad (38)$$

is the coupling of the vertex $V^* \cdot l \cdot \bar{l}$ with $j = \{L, R\}$, $P_{L,R} = \frac{1 \mp \gamma_5}{2}$. In addition, $Q_l = -1$, $I_{3,l}^L = 1/2, I_{3,l}^R = 0$ for $l \equiv e, \mu$; and $Q_l = 0$, $I_{3,l}^L = -1/2, I_{3,l}^R = 0$ for $l \equiv \nu_{e,\mu,\tau}$. Each one-loop form factor $F_{\gamma V^*}^{V^*\text{-pole}}$ is decomposed into three parts as follows

$$F_{\gamma V^*}^{V^*\text{-pole}} = \frac{e^2 g}{(4\pi)^2 M_W} \frac{1}{q_{12} - M_V^2 + iM_V \Gamma_V} \left[F_{\gamma V^*}^{(f)} + F_{\gamma V^*}^{(W)} + F_{\gamma V^*}^{(S)} \right], \quad (39)$$

where M_V , Γ_V are mass and decay width of the gauge boson V^* , and $q_{12} = (q_1 + q_2)^2$. Here, we include all contributions from fermion exchanges f in the loops, namely

$$F_{\gamma V^*}^{(f)} = \sum_f \frac{N_f^C m_f v}{(2\pi\alpha)(m_h^2 - q_{12})^2} g_{hf\bar{f}}^{\text{NP}} g_{\gamma f\bar{f}}^L (g_{V^* f\bar{f}}^L + g_{V^* f\bar{f}}^R) \times \quad (40)$$

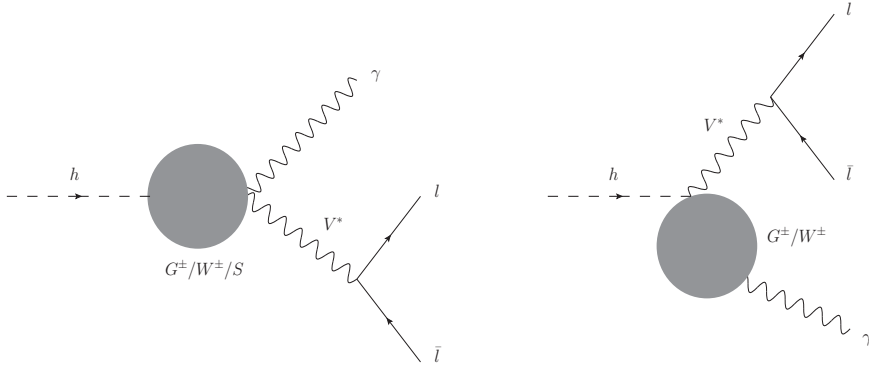


Figure 3: One-loop Feynman diagrams for the decay $h \rightarrow l\bar{l}\gamma$ in group 1.

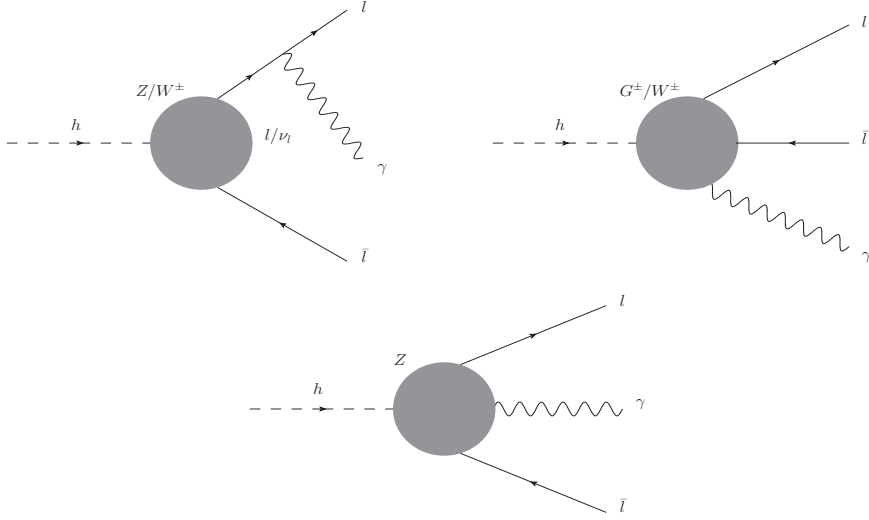


Figure 4: One-loop Feynman diagrams for the decays $h \rightarrow l\bar{l}\gamma$ classifying into group 2.

$$\times \left\{ 2q_{12} \left[B_0(m_h^2, m_f^2, m_f^2) - B_0(q_{12}, m_f^2, m_f^2) \right] \right. \\ \left. + (m_h^2 - q_{12}) \left[2 + (q_{12} - m_h^2 + 4m_f^2) C_0(0, q_{12}, m_h^2, m_f^2, m_f^2, m_f^2) \right] \right\}.$$

Here $g_{\gamma f\bar{f}}^{L,R}$ and $g_{V^* f\bar{f}}^{L,R}$ are the couplings of photon and V^* to fermions, respectively.

Regarding the W exchange in the loop diagrams, we know that there are also involved Nambu-Goldstone bosons, and Ghost exchanges in the loop within the HF gauge. In order to find out a representation which are valid for both $V^* = Z^*$ and γ^* , one adds the parameters δ_{V^*W} and δ_{V^*G} to the couplings of V^* with W bosons, Goldstone bosons and Ghost particles as in Table 5. Subsequently, one-loop form factors for this contribution are given in the compact form as

$$F_{\gamma V^*}^{(W)} = \frac{g_{hWW}^{\text{NP}} v}{2M_W^2 (m_h^2 - q_{12})^2} \left\{ 2M_W^2 (m_h^2 - q_{12}) \left[(\delta_{V^*G} - 5\delta_{V^*W})(m_h^2 - 2M_W^2) \right. \right. \\ \left. \left. - 2q_{12}(\delta_{V^*G} - 3\delta_{V^*W}) \right] C_0(0, q_{12}, m_h^2, M_W^2, M_W^2, M_W^2) \right. \\ \left. - \left[\delta_{V^*G}(m_h^2 + 2M_W^2) - \delta_{V^*W}(m_h^2 + 10M_W^2) \right] \times \right. \quad (41)$$

Vertices	Couplings
g_{V^*WW}	$\delta_{V^*W} e$
g_{V^*WG}	$\delta_{V^*G} (-eM_W)$
$g_{V^*u^\pm u^\mp}$	$\mp \delta_{V^*W} e$
$g_{V^*G^\pm G^\mp}$	$\frac{e}{2} (\delta_{V^*W} - \delta_{V^*G})$

Table 5: Generalizations of the couplings of $V^* = Z^*$ and γ^* to W , G^\pm , and the Ghost particle G in the HF gauge.

$$\times \left[q_{12} \left(B_0(m_h^2, M_W^2, M_W^2) - B_0(q_{12}, M_W^2, M_W^2) \right) + (m_h^2 - q_{12}) \right] \Bigg\}.$$

The mentioned parameters are taken for Z^* -pole and γ^* -pole as follows:

$$\delta_{V^*W}; \delta_{V^*G} = \begin{cases} -1; 1 & \text{if } V^* \equiv \gamma^*, \\ \frac{c_W}{s_W}; \frac{s_W}{c_W} & \text{if } V^* \equiv Z^*. \end{cases} \quad (42)$$

It is worth to mention that we have a full set of gauge invariance Feynman diagrams for each V^* -pole contribution in the HF gauge. Hence, we can derive the above results to many of well-known expressions for $h \rightarrow \gamma\gamma, Z\gamma$ by considering the final state as $V^* \rightarrow Z, \gamma$, respectively. For this purpose, the PV-functions B_0 and C_0 appearing in the above one-loop form factors can be expressed via the basic I_k functions (for $k = 1, 2$) [93] as follows:

$$C_0(0, q_{12}, m_h^2, M_i^2, M_i^2, M_i^2) = -\frac{I_2(\tau_i, \lambda_i)}{M_i^2}, \quad (43)$$

$$B_0(m_h^2, M_i^2, M_i^2) - B_0(q_{12}, M_i^2, M_i^2) = \frac{m_h^2 - q_{12}}{2M_i^2 q_{12}} \left\{ 2M_i^2 \left[2I_2(\tau_i, \lambda_i) - 1 \right] + (q_{12} - m_h^2) I_1(\tau_i, \lambda_i) \right\}, \quad (44)$$

where $\tau_i = 4M_i/m_h^2$ and $\lambda_i = 4M_i^2/q_{12}$. The reductions for $h \rightarrow \gamma\gamma, Z\gamma$ with on-shell Z and photon in final states are presented in the following paragraphs.

- γ^* -pole contributions:

In case of γ^* -pole contributions, taking a limit of M_{V^*} tends to zero as well as the corresponding couplings in Eq. (38) and selecting the appropriated parameters in (42), one-loop form factors $F_{\gamma\gamma^*}^{(f,W)}$ are casted into the form of

$$F_{\gamma\gamma^*}^{(f,W)} = F_{\gamma\gamma^*}^{(f)} + F_{\gamma\gamma^*}^{(W)} = \sum_f N_f^C Q_f^2 F_{\gamma\gamma^*}^{(1/2)}(\tau_f, \lambda_f) + F_{\gamma\gamma^*}^{(1)}(\tau_W, \lambda_W). \quad (45)$$

Where form factors $F_{\gamma\gamma^*}^{(1)}, F_{\gamma\gamma^*}^{(1/2)}$ are taken into account in the above equation as follows:

$$F_{\gamma\gamma^*}^{(1)}(\tau_W, \lambda_W) = 16 I_2(\tau_W, \lambda_W) - (4/\tau_W + 6) I_1(\tau_W, \lambda_W), \quad (46)$$

$$F_{\gamma\gamma^*}^{(1/2)}(\tau_f, \lambda_f) = 4I_1(\tau_f, \lambda_f) - 4I_2(\tau_f, \lambda_f). \quad (47)$$

For the decay $h \rightarrow \gamma\gamma$ corresponding to the limit of $q_{12} \rightarrow 0$, we derived once again the SM results shown in Ref. [29].

- Z^* -pole contributions:

Similarly, in the Z^* -pole contributions with $M_{V^*} = M_Z$, and $\Gamma_{V^*} = \Gamma_Z$, the respective one-loop form factor $F_{\gamma Z^*}^{(f,W)}$ is:

$$F_{\gamma Z^*}^{(f,W)} = F_{\gamma Z^*}^{(f)} + F_{\gamma Z^*}^{(W)} = \sum_f N_f^C \frac{Q_f v_f}{s_W c_W} F_{\gamma Z^*}^{(1/2)}(\tau_f, \lambda_f) + F_{\gamma Z^*}^{(1)}(\tau_W, \lambda_W), \quad (48)$$

where $v_f = 2I_3^f - 4Q_f s_W^2$, and

$$F_{\gamma Z^*}^{(1)}(\tau_W, \lambda_W) = \frac{c_W}{s_W} \left\{ \left[\left(\frac{2}{\tau_W} + 1 \right) \frac{s_W^2}{c_W^2} - \left(\frac{2}{\tau_W} + 5 \right) \right] I_1(\tau_W, \lambda_W) + 4 \left(3 - \frac{s_W^2}{c_W^2} \right) I_2(\tau_W, \lambda_W) \right\},$$

$$F_{\gamma Z^*}^{(1/2)}(\tau_f, \lambda_f) = I_1(\tau_f, \lambda_f) - I_2(\tau_f, \lambda_f). \quad (49)$$

The decay process $h \rightarrow Z\gamma$ corresponds to $q_{12} = M_Z^2$, leading to the SM results presented in Refs. [30, 31].

We turn our attention to the case of a Higgs boson S exchanging in the loop of a diagram, which gives the one-loop form factor $F_{\gamma V^*}^{(S)}$ determined as follows

$$F_{\gamma V^*}^{(S)} = \frac{4M_W}{g(m_h^2 - q_{12})^2} \sum_S Q_S^2 g_{hSS}^{(NP)} g_{ASS}^{(NP)} g_{VSS}^{(NP)} \left\{ q_{12} \left[B_0(m_h^2, M_S^2, M_S^2) - B_0(q_{12}, M_S^2, M_S^2) \right] + (m_h^2 - q_{12}) \left[2M_S^2 C_0(0, q_{12}, m_h^2, M_S^2, M_S^2, M_S^2) + 1 \right] \right\}, \quad (50)$$

where Q_S is the electric charge of S . Any neutral Higgs bosons S with $Q_S = 0$ do not contribute to $F_{\gamma V^*}^{(S)}$. The decay processes $h \rightarrow V\gamma$ have amplitudes with one-loop form factors derived from $F_{\gamma V}^{(S)}$ as follows

$$F_{\gamma\gamma}^{(S)} = \frac{4M_W}{gm_h^2} \sum_S Q_S^2 g_{hSS}^{(NP)} \left[g_{ASS}^{(NP)} \right]^2 \left[2M_S^2 C_0(0, 0, m_h^2, M_S^2, M_S^2, M_S^2) + 1 \right], \quad (51)$$

$$F_{\gamma Z}^{(S)} = \frac{4M_W}{g(m_h^2 - M_Z^2)^2} \sum_S Q_S^2 g_{hSS}^{(NP)} g_{ASS}^{(NP)} g_{ZSS}^{(NP)} \left\{ M_Z^2 \left[B_0(m_h^2, M_S^2, M_S^2) - B_0(M_Z^2, M_S^2, M_S^2) \right] + (m_h^2 - M_Z^2) \left[2M_S^2 C_0(0, M_Z^2, m_h^2, M_S^2, M_S^2, M_S^2) + 1 \right] \right\}. \quad (52)$$

The above form factors can be written via the well-known I_k functions for $k = 1, 2$ [93], namely:

$$F_{\gamma\gamma}^{(S)} = \frac{M_W}{g} \sum_S Q_S^2 \frac{g_{hSS}^{(NP)} [g_{ASS}^{(NP)}]^2}{M_S^2} \tau_S \left[1 - \tau_S f(\tau_S) \right], \quad (53)$$

$$F_{\gamma Z}^{(S)} = -\frac{M_W}{2g} \sum_S Q_S^2 \frac{g_{hSS}^{(NP)} g_{ASS}^{(NP)} g_{ZSS}^{(NP)}}{M_S^2} \tau_S I_1(\tau_S, \rho_S), \quad (54)$$

where $\tau_S = 4M_S^2/m_h^2$, $\rho_S = 4M_S^2/M_Z^2$, and all analytic expressions of the basis functions $I_1(x, y)$, $I_2(x, y)$ and $f(z)$ are shown given in [Appendix D](#).

We also give several interesting comments on our results as follows. First, summing of all γ^* -contributions, we can derive the results for $h \rightarrow \gamma\gamma$ in many EHSM, for examples, the IDM [51], THM [75], and a class of EHSM [60]. For $h \rightarrow Z\gamma$ in many of EHSM [60, 61, 72, 80], we can select all the contributions from Z^* -pole. Our formulas confirm again the previous results for many EHSM.

3.2. Non-pole V -contributions

The non-pole contributions come from the Feynman diagrams in group 2. There are many kinds of Feynman diagrams which are involed to vector W, Z bosons, their Goldstone bosons and the cases of scalar Higgs exchanging, mixing of vector boson and scalar Higgs in the loop diagrams. The later give much smaller contributions than the former due to the appearance of the couplings $S\bar{l}l$ proportional to m_l . Therefore, we ignore all contributions from diagrams having this kind of couplings. The remaining ones can be divided into two parts. The first (second) part includes Z (W) and its Goldstone boson in the loop diagrams, respectively. One-loop amplitude is given

$$\mathcal{A}_{\text{Non-pole, V}} = \sum_{V=\{Z,W,S\}} \sum_{k=1}^2 \left\{ [q_3^\mu q_k^\nu - g^{\mu\nu} q_3 \cdot q_k] \bar{u}(q_1) \left(\sum_{j=L,R} F_{k,j}^{\text{Non-pole, V}} \gamma_\mu P_j \right) v(q_2) \right\} \varepsilon_\nu^*(q_3). \quad (55)$$

As we have pointed out in above arguments that the contributions of S in the loop diagrams can be obmited. It is enough to consider Z, W exchanging in the loop diagrams. In the first contribution, we concern one-loop diagrams with Z boson internal lines. One loop form factors are written in terms of scalar PV-functions as follows:

$$F_{1,L}^{\text{Non-pole, Z}} = \frac{\alpha v g_{hZZ}^{\text{NP}} (g_{Zl\bar{l}}^L)^2}{\pi M_Z s_{2W}} \left[D_2 + D_{12} + D_{23} \right] (0, q_{13}, m_h^2, q_{23}, 0, 0, m_l^2, m_l^2, M_Z^2, M_Z^2), \quad (56)$$

$$F_{1,R}^{\text{Non-pole, Z}} = F_{1,L}^{\text{Non-pole, Z}} \Big|_{g_{Zl\bar{l}}^L \rightarrow g_{Zl\bar{l}}^R}, \quad (57)$$

$$F_{2,L}^{\text{Non-pole, Z}} = F_{1,L}^{\text{Non-pole, Z}} \Big|_{q_{13} \leftrightarrow q_{23}}, \quad (58)$$

$$F_{2,R}^{\text{Non-pole, Z}} = F_{2,L}^{\text{Non-pole, Z}} \Big|_{g_{Zl\bar{l}}^L \rightarrow g_{Zl\bar{l}}^R}, \quad (59)$$

where $q_{13} = (q_1 + q_3)^2$, $q_{23} = (q_2 + q_3)^2$. Changing into the forms of scalar integrals, we have

$$\begin{aligned} F_{1,L}^{\text{Non-pole, Z}} &= \frac{\alpha v}{2\pi} \frac{g_{hZZ}^{\text{NP}} (g_{Zl\bar{l}}^L)^2}{M_Z s_{2W} q_{12} q_{13}^2 (q_{12} + q_{13})} \frac{q_{23}}{q_{23} - m_l^2} \times \\ &\times \left\{ 2q_{12}q_{13} \left[B_0(m_h^2, M_Z^2, M_Z^2) - B_0(q_{23}, 0, M_Z^2) \right] \right. \\ &- \left[M_Z^2 (q_{12}^2 + 2q_{12}q_{13} - q_{13}^2) + (q_{13}^2 - q_{12}^2)q_{13} \right] C_0(0, m_h^2, q_{23}, 0, M_Z^2, M_Z^2) \\ &- q_{23}(M_Z^2 - q_{13})(q_{12} + q_{13})C_0(0, 0, q_{23}, 0, 0, M_Z^2) \\ &+ (m_h^2 - q_{13})(M_Z^2 - q_{13})(q_{12} + q_{13})C_0(q_{13}, m_h^2, 0, 0, M_Z^2, M_Z^2) \\ &+ q_{13}(q_{13} - M_Z^2)(q_{12} + q_{13})C_0(0, q_{13}, 0, 0, 0, M_Z^2) \\ &\left. - (M_Z^2 - q_{13})(q_{12} + q_{13}) \left[m_h^2(M_Z^2 - q_{13}) - M_Z^2 q_{12} + q_{13}(q_{12} + q_{13}) \right] \right\} \times \end{aligned} \quad (60)$$

$$\times D_0(0, q_{13}, m_h^2, q_{23}, 0, 0, 0, 0, M_Z^2, M_Z^2) \Big\}.$$

We next arrive at the non-pole W -contributions described in Fig. 4. The one-loop amplitude is the same as that in (55) with the following form factors:

$$F_{1,L}^{\text{Non-pole, W}} = -\frac{\alpha^2 v g_{hWW}^{\text{NP}}}{2 M_W s_W^3} \left\{ \left[D_1 + D_{13} \right] (0, q_{12}, 0, q_{23}, 0, m_h^2, 0, M_W^2, M_W^2, M_W^2) \right. \quad (61)$$

$$\left. + \left[D_2 - D_{23} - D_{33} \right] (0, q_{12}, 0, q_{13}, 0, m_h^2, 0, M_W^2, M_W^2, M_W^2) \right\},$$

$$F_{1,R}^{\text{Non-pole, W}} = F_{2,R}^{\text{Non-pole, W}} = 0, \quad (62)$$

$$F_{2,L}^{\text{Non-pole, W}} = F_{1,L}^{\text{Non-pole, W}} \Big|_{q_{13} \leftrightarrow q_{23}}. \quad (63)$$

$F_{k,R}^{\text{Non-pole, W}} = 0$ with $k = 1, 2$ because the W boson only couples to left-handed neutrinos. The expression of non-pole W -boson contributions in terms of one-loop scalar integrals are:

$$F_{1,L}^{\text{Non-pole, W}} = \frac{\alpha^2 v g_{hWW}^{\text{NP}}}{2 M_W s_W^3} \frac{q_{23}}{q_{12}(q_{12} + q_{13})q_{13}^2 q_{23} - m_l^2} \times \quad (64)$$

$$\times \left\{ -2q_{12}q_{13} \left[B_0(m_h^2, M_W^2, M_W^2) - B_0(q_{23}, 0, M_W^2) \right] \right.$$

$$- (q_{12}^2 + 2q_{12}q_{13} - q_{13}^2)(-M_W^2 + q_{12} + q_{13})C_0(0, m_h^2, q_{23}, 0, M_W^2, M_W^2)$$

$$+ q_{12}^2(q_{12} + q_{13})C_0(0, q_{12}, 0, 0, M_W^2, M_W^2)$$

$$+ q_{23}(q_{12} + q_{13})(-M_W^2 + q_{12} + q_{13})C_0(0, 0, q_{23}, 0, M_W^2, M_W^2)$$

$$- q_{13}(M_W^2 - q_{13})(q_{12} + q_{13})C_0(0, 0, q_{13}, 0, M_W^2, M_W^2)$$

$$+ (m_h^2 - q_{13})(q_{13} - M_W^2)(q_{12} + q_{13})C_0(0, m_h^2, q_{13}, 0, M_W^2, M_W^2)$$

$$- (m_h^2 - q_{12})(q_{12} + q_{13})(-2M_W^2 + q_{12} + 2q_{13})C_0(q_{12}, 0, m_h^2, M_W^2, M_W^2, M_W^2)$$

$$- (q_{12} + q_{13}) \left[q_{13}M_W^2(M_W^2 + q_{12} - q_{13}) \right.$$

$$\left. + (M_W^2 - q_{12})(M_W^2 - q_{12} - q_{13}) \right] D_0(0, q_{12}, 0, q_{23}, 0, m_h^2, 0, M_W^2, M_W^2, M_W^2)$$

$$- (M_W^2 - q_{13})(q_{12} + q_{13}) \left[m_h^2 M_W^2 + q_{12}(q_{13} - M_W^2) \right] \times$$

$$\left. \times D_0(0, q_{12}, 0, q_{13}, 0, m_h^2, 0, M_W^2, M_W^2, M_W^2) \right\}.$$

The analytic expressions of the PV-fuction C_0 , D_0 are then written in terms of the logarithm and the di-logarithmic functions as given in Appendix B.

The total one-loop form factors are computed as follows:

$$F_{k,L/R} = \sum_{V^*=\{\gamma^*, Z^*\}} g_{V^*l}^{L/R} \cdot F_{\gamma V^*}^{V^*\text{-pole}} + \sum_{V=\{Z, W\}} F_{k,L/R}^{\text{Non-pole, V}} \quad (65)$$

for $k = 1, 2$.

We first check our calculations by testing the independent of the UV -divergent, IR -divergent, μ^2 -independent of the form factors. We also cross-check the decay rates to our previous work

and other references if they are available [24, 28, 32]. For these decay processes, we have no IR -divergent. Since we don't have photon exchange in the loop diagrams. For UV -divergence, μ^2 -independence checking analytically, we refer Appendix C for more details. Numerical checks our work with other papers and our previous works will be shown in the next section. We confirm the correctness of the calculations.

Having the correctness form factors for the decay processes, the decay rate is given by [24]:

$$\frac{d\Gamma}{dq_{12}q_{13}} = \frac{q_{12}}{512\pi^3 m_h^3} \left[q_{13}^2 (|F_{1,R}|^2 + |F_{2,R}|^2) + q_{23}^2 (|F_{1,L}|^2 + |F_{2,L}|^2) \right]. \quad (66)$$

Taking the above integrand over $(m_{ll}^{\text{cut}})^2 \leq q_{12} \leq m_h^2$ and $0 \leq q_{13} \leq m_h^2 - q_{12}$, one gets the total decay rates. For our later discussions, we define the standard formula for the enhancement factor of the decay rates as follows:

$$R_{\text{NP}}(\mathcal{P}_{\text{NP}}) = \frac{\Gamma_{h \rightarrow l\bar{l}\gamma}^{\text{NP}}(\mathcal{P}_{\text{NP}})}{\Gamma_{h \rightarrow l\bar{l}\gamma}^{\text{SM}}}, \quad (67)$$

where $\Gamma_{h \rightarrow l\bar{l}\gamma}^{\text{NP}}(\mathcal{P}_{\text{NP}})$ (and $\Gamma_{h \rightarrow l\bar{l}\gamma}^{\text{SM}}$) is the decay rate of the EHSM and SM, respectively.

We also interested in the fermion FB asymmetry in $h \rightarrow l\bar{l}\gamma$, which is defined through the following integrated FB asymmetry:

$$\mathcal{A}_{\text{FB}}(\mathcal{P}_{\text{NP}}) = \frac{\int_{E_\gamma^{\text{cut}}}^{m_h/2} \int_0^1 \frac{d\Gamma}{dE_\gamma d\cos\theta_l} d\cos\theta_l dE_\gamma - \int_{E_\gamma^{\text{cut}}}^{m_h/2} \int_{-1}^0 \frac{d\Gamma}{dE_\gamma d\cos\theta_l} d\cos\theta_l dE_\gamma}{\int_{E_\gamma^{\text{cut}}}^{m_h/2} \int_0^1 \frac{d\Gamma}{dE_\gamma d\cos\theta_l} d\cos\theta_l dE_\gamma + \int_{E_\gamma^{\text{cut}}}^{m_h/2} \int_{-1}^0 \frac{d\Gamma}{dE_\gamma d\cos\theta_l} d\cos\theta_l dE_\gamma}, \quad (68)$$

where E_γ , $\cos\theta_l$ are the energy of photon and cosine angle between two momentum directions of photon and lepton in the rest frame of the SM-like Higgs boson. The energy cut for photon is $E_\gamma^{\text{cut}} \geq 4m_l^2$. We refer Appendix E for the details of kinematic and phase space of $1 \rightarrow 3$ in the rest frame of the SM-like Higgs boson.

4. Phenomenological results

For numerical investigation, we will use the following input parameters: $M_Z = 91.1876$ GeV, $\Gamma_Z = 2.4952$ GeV, $M_W = 80.379$ GeV, $\Gamma_W = 2.085$ GeV, $m_h = 125.1$ GeV, $\Gamma_h = 4.07 \cdot 10^{-3}$ GeV. For lepton masses we take $m_e = 0.00052$ GeV, $m_\mu = 0.10566$ GeV and $m_\tau = 1.77686$ GeV. All quark masses are $m_u = 0.00216$ GeV, $m_d = 0.0048$ GeV, $m_c = 1.27$ GeV, $m_s = 0.93$ GeV, $m_t = 173.0$ GeV, and $m_b = 4.18$ GeV. We are working in the so-called G_μ -scheme, where the Fermi constant is an input parameter with $G_\mu = 1.16638 \cdot 10^{-5}$ GeV⁻². The electroweak constant is then calculated appropriately as follows:

$$\alpha = \sqrt{2}/\pi G_\mu M_W^2 (1 - M_W^2/M_Z^2) = 1/132.184. \quad (69)$$

The inputs for scanning parameters will be presented corresponding to particular HESM models.

We first cross-check numerically the results obtained in this work with our previous paper [28] and other references [24]. We take the THDM (type I or X) as an illustration. In the first column of Table 6, the singly charged Higgs mass changes from 400 GeV to 1000 GeV. In this test, we take $t_\beta = 10$, $\alpha = 0.4\pi$, apply the cut of the invariant mass of lepton-pair as $m_{ll}^{\text{cut}} = k_{\text{cut}} m_h$ with $k_{\text{cut}} = 0.1$. The second and third columns present the two numerical results evaluated in this work and Ref. [28], respectively. We find that the two results are in good agreement (more than

M_{H^\pm} [GeV]	Γ [KeV]	Ref. [28]
400	6.157263708843869	6.157263708844675
600	1.097388878039453	1.097388878039259
800	0.304842878283716	0.304842878276348
1000	0.105534527108802	0.105534527102357

Table 6: $t_\beta = 10$, $\alpha = 0.4\pi$ and $k_{\text{cut}} = 0.1$. Decay rate in KeV.

13 digits), confirming that two results are consistent when they are calculated in different gauges. Therefore, the test relies on gauge invariance of the processes. A cross-checking the integrated FB asymmetries $\mathcal{A}_{\text{FB}}^{(l)}$ for $l = e, \mu$ with the ones in [24] in the SM framework is presented in Table 7. In this test we use the cuts $m_{ll}^{\text{cut}} = 0.1m_h$ and $E_\gamma^{\text{cut}} = 5$ GeV. We find that our results

$\mathcal{A}_{\text{FB}}^{(l)}$	This work	Ref. [24]
$\mathcal{A}_{\text{FB}}^{(e)}$	0.3673	0.366
$\mathcal{A}_{\text{FB}}^{(\mu)}$	0.2843	0.280

Table 7: Cross-checking the integrated FB asymmetries $\mathcal{A}_{\text{FB}}^{(l)}$ for $l = e, \mu$ over full phase-space with [24] in the SM framework.

are good agreement with the corresponding ones in [24].

Before going to discuss phenomenological results for HESM, we note that for the study of the enhancement factors, the cuts of $m_{ll}^{\text{cut}} = 0.1m_h$ are applied. Furthermore, once we consider the FB asymmetries of fermions, we apply a further cut for external photon as $E_\gamma^{\text{cut}} = 5$ GeV.

4.1. The IDM

For our analysis, we first review the current constraints on the scanning set of parameters given in Eq. (7). The experimental constraints including Electroweak Precision Tests (EWPT) of the IDM, Dark matter search at the LHC, and LEP data were given in Refs. [49, 50, 51, 52]. The loop-induced decays were also studied in the IDM framework, for example $h \rightarrow \gamma\gamma$ [53, 60, 61], and $h \rightarrow Z\gamma$ [60, 61]. Benchmarks for searching signals of the IDM at future colliders were discussed in Ref. [54, 55, 56, 57, 58, 59]. The theoretical and experimental constraints on these parameters were also studied in the above papers, where the most important theoretical constraints must ensure the tree-level unitarity, vacuum stability, perturbativity regime, giving strict constraints on the Higgs self couplings λ_i for $i = 1, 2, \dots, 5$ and μ_2 . Taking into account all constraints mentioned in the above works, it is reasonable to choose the ranges of parameters as follows: $5 \text{ GeV} \leq M_H \leq 150 \text{ GeV}$, $70 \text{ GeV} \leq M_{H^\pm}, M_{A^0} \leq 1000 \text{ GeV}$, $|\mu_2| \leq 500 \text{ GeV}$, and $0 \leq \lambda_2 \leq 8\pi$.

Fig. 5 shows a scatter plot of the enhancement factor as a function of the charged Higgs mass M_{H^\pm} and μ_2 . There exist large deviations of the enhancement factor R_{IDM} from 1, which corresponds to the SM limit, for $70 \text{ GeV} \leq M_{H^\pm} \leq 500 \text{ GeV}$, but in the whole scanning range $-500 \leq \mu_2 \leq 500$. Moreover, R_{IDM} depends strongly on μ_2 parameter for $M_{H^\pm} \leq 500 \text{ GeV}$. It is interesting to observe that R_{IDM} tends to ~ 0.95 with heavy values of singly charged Higgs mass, implying that the factor is not sensitive with μ_2 . In the region of $M_{H^\pm} \geq 500 \text{ GeV}$,

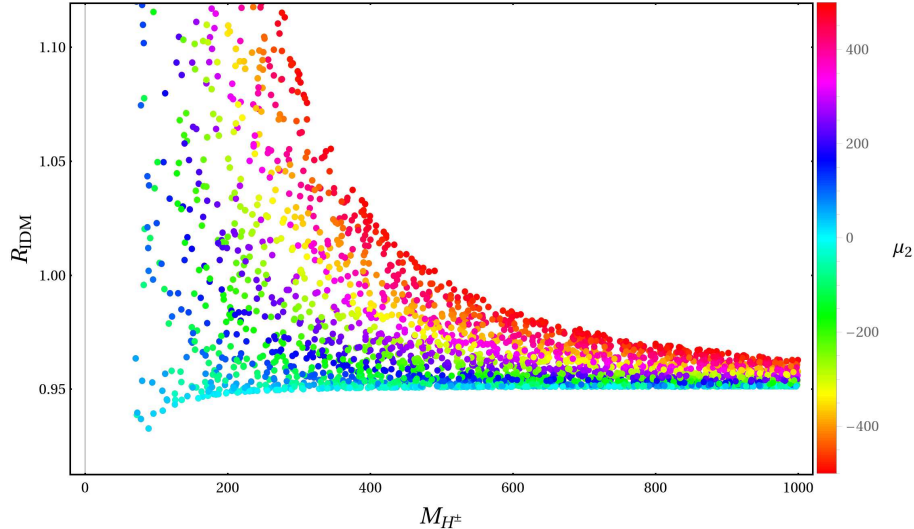


Figure 5: The enhancement factor as function of charged Higgs mass M_{H^\pm} and μ_2 is shown.

the contributions of charged Higgs exchange ($\sim 5\%$) are smaller than other ones. With high-luminosity of future colliders, the IDM effect could be tested. The plot provides a key role to probe indirect effect of the charged Higgs boson at future colliders.

In Table 8, the FB asymmetries of fermions are presented as a functions of M_{H^\pm} and μ_2 . We change the values of M_{H^\pm} , μ_2 in the first column, by accessing all possible values in the scanning ranges. Consequently, the second and third columns show numerical values of the FB asymmetries of electron and muon, respectively. It can be seen that these FB asymmetries get contribution mainly from the interference of the Z^* -pole diagrams with the remaining ones. In this model, only more diagrams with singly charged Higgs exchange appear. However, their contributions are smaller than those observed in the enhancement factor plot, resulting that we get nearly same results of FB asymmetries of fermions as those predicted by the SM.

4.2. THDM

Following the same strategies for phenomenological studies in many of BSMs, one first summarizes the theoretical and experimental constraints on the scanning parameters in THDM. Theoretical constraints subject to the tree-level unitarity, vacuum stability, perturbativity regime were shown in Ref. [63, 64, 65, 66, 68], giving strict bounds on λ_i for $i = 1, 2, \dots, 5$ and m_{11}, m_{12}, m_{22} . The experimental constraints are obtained from the EWPT of THDM, implying the LEP data [69, 70]. Furthermore, direct and indirect searching for scalar masses in THDM were reported from LEP, Tevaron and the LHC [67]. Implications for loop-induced decays of $h \rightarrow \gamma\gamma$ and $h \rightarrow Z\gamma$ were presented in Refs. [53, 60, 61]. Combining all the constraints, we scan consistently the input parameters for THDM as follows. In the type-I and X: we take $126 \text{ GeV} \leq M_H \leq 1000 \text{ GeV}$, $60 \text{ GeV} \leq M_{A^0} \leq 1000 \text{ GeV}$ and $80 \text{ GeV} \leq M_{H^\pm} \leq 1000 \text{ GeV}$. In the Type-II and Y: we scan logically the physical parameters as $500 \text{ GeV} \leq M_H \leq 1000 \text{ GeV}$, $500 \text{ GeV} \leq M_{A^0} \leq 1000 \text{ GeV}$ and $580 \text{ GeV} \leq M_{H^\pm} \leq 1500 \text{ GeV}$. In both types, one takes $2 \leq t_\beta \leq 20$, $0.95 \leq s_{\beta-\alpha} \leq 1$ and $m_{12}^2 = M_H^2 s_\beta c_\beta$.

In Fig. 6, we analysis the enhancement factors as functions of t_β and neutral Higgs mass M_H for four types of THDM, fixing $s_{\beta-\alpha} = 0.95$, and $M_{H^\pm} = 800 \text{ GeV}$. The scanning ranges of t_β and M_H are $2 \leq t_\beta \leq 20$ and $126 \text{ GeV} \leq M_H \leq 1000 \text{ GeV}$ for types I and X, and $500 \text{ GeV} \leq M_H \leq 1000 \text{ GeV}$ for types II and Y. The two models types I and X predict that the enhancement factors tend to 0.9 when $M_H \leq 400 \text{ GeV}$. Beyond this region, namely with

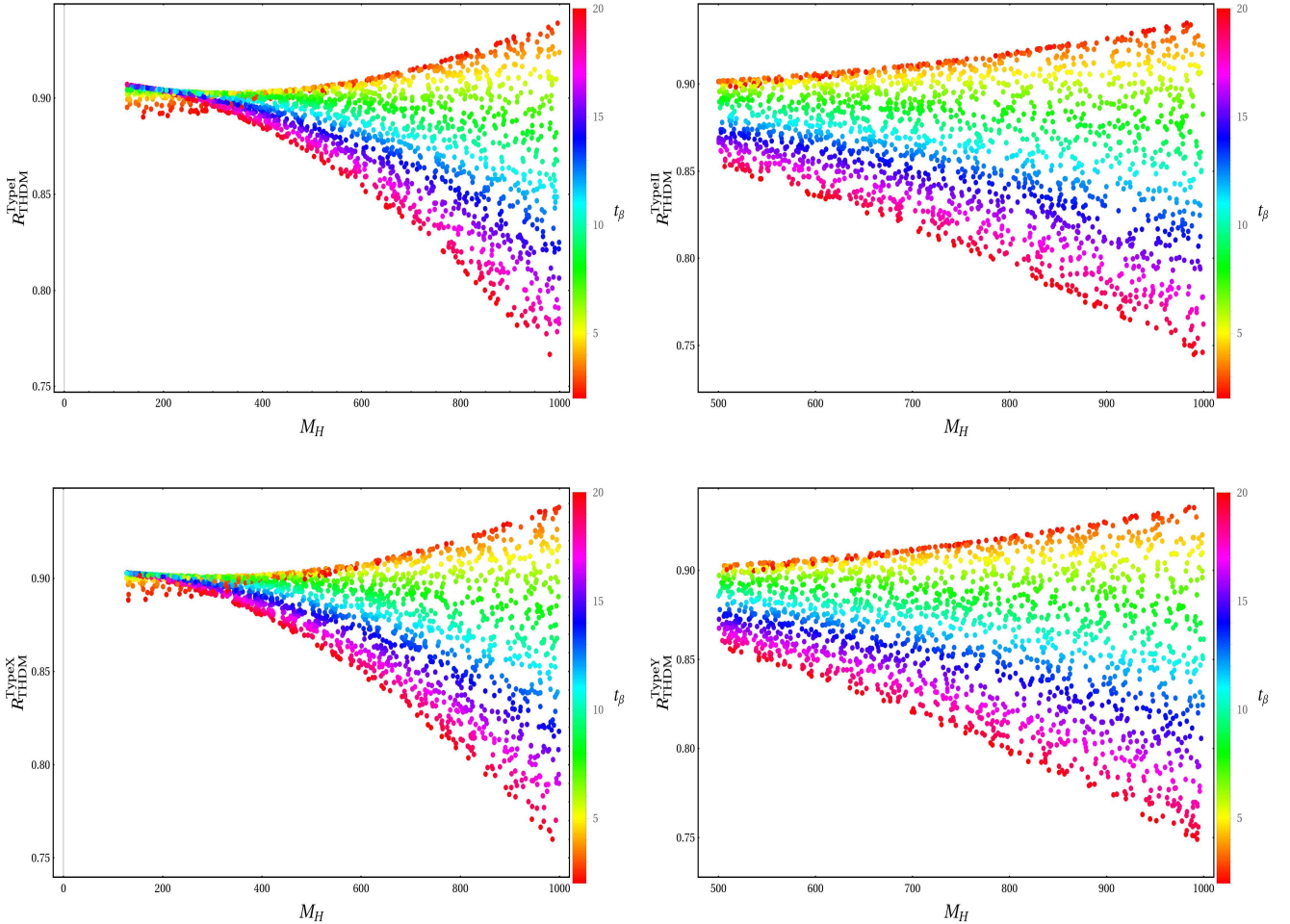


Figure 6: The enhancement factors R_{THDM} as functions of t_β and M_H for four types of the THDM.

$M_H \geq 400$ GeV, R_{THDM} are sensitive with both t_β and m_H , which give large deviations of the decay rates between all four THDM types and the SM. It is stressed that the enhancement factors in the two THDM types I and X are slightly different from those of types II and Y, which results from the properties of Yukawa couplings giving smaller contributions than those obtained from the W boson exchange.

Fig. 7 shows the enhancement factors as functions of M_{H^\pm} and $s_{\beta-\alpha}$, where $t_\beta = 15$ and $M_H = 1000$ GeV are selected. It observes that the enhancement factors of the two THDM types I and X have the same behavior, which also happens in the two THDM types II and Y. As discussed previously, the slightly different values of the enhancement factors between the two classes of THDM types (I, X) and (II, Y) originate from the Yukawa couplings. In the THDM types I and X, the enhancement factors have wide deviations from 1 in the region $M_{H^\pm} \leq 600$ GeV. In addition, these factors are more sensitive with $s_{\beta-\alpha}$ in smaller values of M_{H^\pm} . In contrast, large $M_{H^\pm} \geq 800$ GeV corresponds to the range $0.85 \leq R_{\text{THDM}} \leq 1.1$, and converge to the values close to 1 with very heavy M_{H^\pm} . In the THDM types II and Y, the enhancement factors have large deviations from 1 in all ranges of M_{H^\pm} and $s_{\beta-\alpha}$. In conclusion, these plots mentioned here show that one may constrain the mixing angle and the singly charged mass at future colliders.

In Table 9, we generate numerical results of the fermion FB asymmetries at several points in the parameter spaces of the THDM types I and X. The parameters $t_\beta, s_{\beta-\alpha}, M_{H^\pm}$ and M_H are selected in such a way to cover all possible values in their scanning ranges mentioned above. The

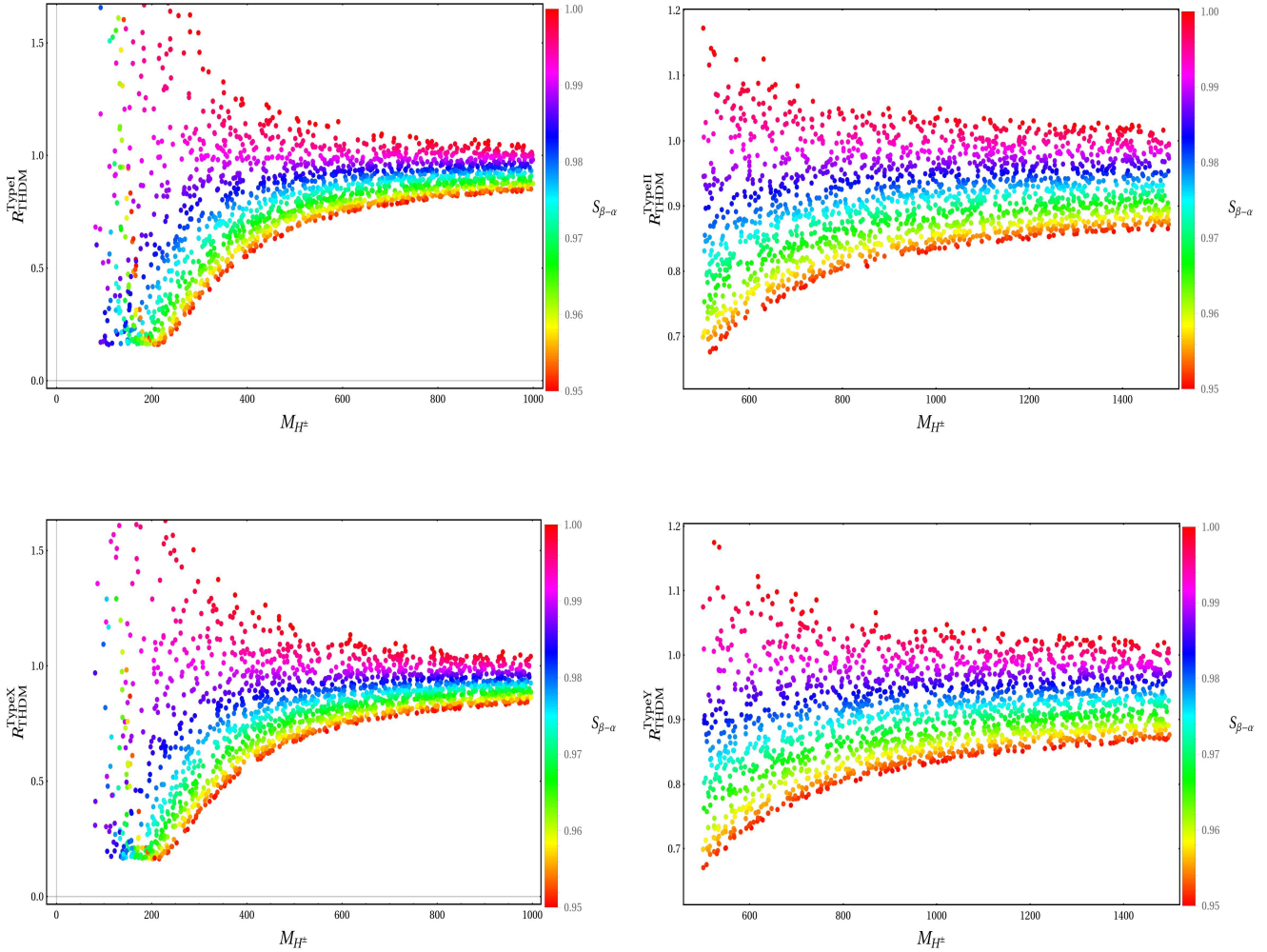


Figure 7: The enhancement factor for four types of THDM.

numerical values of these parameters are shown in the first column of Table 9. In the second (third) column, we report the values of the FB asymmetries (enclosed with the enhancement factors) of electron and muon, respectively. The results are presented for THDM type I (first line data) and X (second line data). The results in this Table should compare with the values of the asymmetries in the SM which are given $\mathcal{A}_{\text{FB}}^{(e)} = 0.3673$ and $\mathcal{A}_{\text{FB}}^{(\mu)} = 0.2843$, accordingly. The data indicates that the enhancement factors and the integrated FB asymmetries are same direction of the derivation to the SM's values. We also find that a bigger derivation of FB asymmetry for muon than the one for electron. It is because we are not considered the tree diagram contributions in both the SM and THDM.

Similarly, Table 10 shows numerical results relating to the two THDM types II and Y, with the same notations defined in Table 9. We have the same conclusions as those derived from the THDMs types I and X. The THDM has only more diagrams with singly charged Higgs exchange in the loop, which give in smaller contributions than the other ones. Therefore, we also have same conclusions for $A_{\text{FB}}^{(l)}$ as in the IDM.

4.3. THM

We arrive at the phenomenological results for the last model in this work. The theoretical and experimental constraints on the mentioned scanning parameters in THM were shown precisely in Refs. [71, 72, 73, 74, 75, 76, 77, 78, 79, 80, 81, 82, 84, 85, 86]. Combining all of these constraints,

it is reasonable to scan the mentioned parameters for the THM in the following ranges: $v_\Delta = 1$ MeV or 5 MeV, $0.95 \leq c_\alpha \leq 1$, $60 \text{ GeV} \leq M_{H^\pm}, M_{H^{\pm\pm}}, M_{A^0}, M_H \leq 1000 \text{ GeV}$.

Since we want to generate scatter plots as functions of λ_1 . The couplings of the SM-like Higgs boson to singly and doubly charged Higgs bosons will be expressed in terms of this parameter. In the scope of this paper, we are concerned the case of $\frac{v_\Delta}{v_\Phi} \ll 1$. When $\frac{v_\Delta}{v_\Phi} \rightarrow 0$, one has $s_{\beta^\pm} \rightarrow 0$ as well as using Eq. (35), the results read

$$g_{hH^\pm H^\mp}^{\text{THM}} = \lambda_1 v_\Phi c_\alpha + \frac{\lambda_4}{2} v_\Phi c_\alpha = \frac{v}{2} (2\lambda_1 + \lambda_4) c_\alpha = \lambda_1 v c_\alpha + \frac{2(M_{A^0}^2 - M_{H^\pm}^2)}{v} c_\alpha, \quad (70)$$

$$g_{hH^{\pm\pm} H^\mp}^{\text{THM}} = \lambda_1 v_\Phi c_\alpha = \lambda_1 v c_\alpha. \quad (71)$$

For our numerical studies, we use the following relation:

$$M_{A^0}^2 = 2M_{H^\pm}^2 - M_{H^{\pm\pm}}^2. \quad (72)$$

The enhancement factor as function of λ_1 , singly (doubly) charged Higgs boson (right panel) are plotted in the left (right) panel of Fig. 8, where $c_\alpha = 0.98$ is fixed and the scanning range of λ_1 is $-6 \leq \lambda_1 \leq 6$. In addition, $M_{H^{\pm\pm}} = 600$ ($M_{H^\pm} = 500$) GeV is fixed in the left (right)

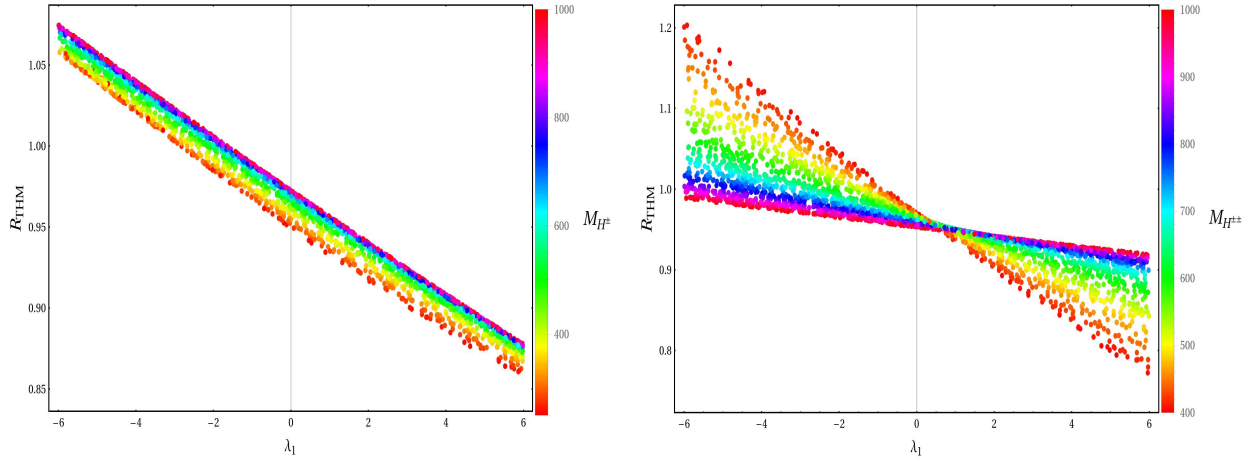


Figure 8: The enhancement factors are functions of λ_1 and singly (left panel) and doubly (right panel) charged Higgs mass.

panel. In the left panel of Fig. 8, we find that the enhancement factor is smaller (larger) than 1 for $\lambda_1 \geq -3$ ($\lambda_1 \leq -3$), and depends nearly linearly on λ_1 . While this factor is not sensitive with M_{H^\pm} . In the right panel, the enhancement factor is greater (smaller) than 1 when $\lambda_1 \leq -1$ ($\lambda_1 \geq -1$) for all values of the doubly charged Higgs mass. With a fixed value of $m_{H^{\pm\pm}}$, this factor develops linearly with λ_1 and gives large deviations from 1 for large $|\lambda_1|$.

We next study the enhancement factor as function of M_{H^\pm} and $M_{H^{\pm\pm}}$ at the two fixed values of $\lambda_1 = \pm 4$ and $c_\alpha = 0.98$, as shown in Fig. 9. In the left panel corresponding to $\lambda_1 = -4$, we find that the enhancement factors have wide deviations from 1 in the region $M^\pm \leq 200 \text{ GeV}$. On the other hand, $0.83 \leq R_{THM} \leq 0.95$ in the region $M^\pm \geq 200 \text{ GeV}$. The results show that the enhancement factors are more sensitive with $M_{H^{\pm\pm}}$ in the region of light M_{H^\pm} . The right panel shows numerical results of the enhancement factor with $\lambda_1 = 4$. At small $M_{H^\pm} \leq \sim 200 \text{ GeV}$, the enhancement factors are much greater than 1 and more sensitive with $M_{H^{\pm\pm}}$. In contrast, the region with of $M_{H^\pm} \geq \sim 200 \text{ GeV}$, the enhancement factors develop in a range of $[0.98, 1.13]$. Two scenarios for different λ_1 can be distinguished from these plots and could be probed at

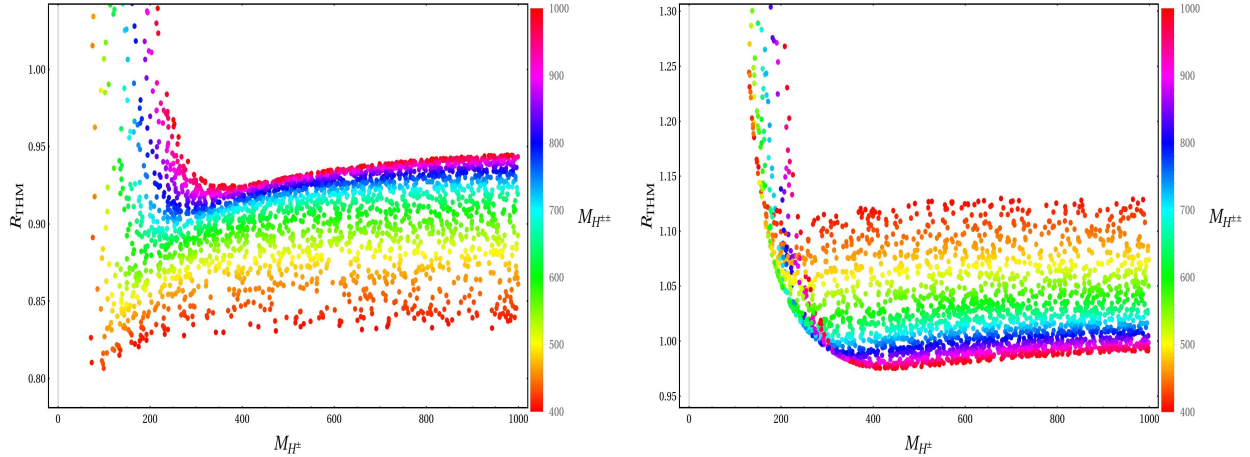


Figure 9: The enhancement factor as a function of M_{H^\pm} and $M_{H^{\pm\pm}}$ with two fixed values of $\lambda_1 = -4$ (4) in the left (right) panel.

future colliders. We also show that the indirect effect of singly and doubly charged Higgs bosons could be probed by measuring these factors in future colliders.

In Table 11, we present the fermion FB asymmetries as functions of singly and doubly charged Higgs masses and λ_1 . The first column list numerical values of M_{H^\pm} , $M_{H^{\pm\pm}}$, and λ_1 with fixed $v_\Delta = 5$ MeV and $c_\alpha = 0.95, 0.98$. The second (third) column shows numerical values of the FB asymmetries of electron (muon). We cover all possible values of M_{H^\pm} , $M_{H^{\pm\pm}}$ in the scanning ranges of the THM discussed above. We obtain the same conclusions with IDM and THDM, except that the THM predicts bigger deviations from the SM result than those predicted by the two models IDM and THDM. Since, we have not only singly and doubly charged Higgs in the loop of Z^* -pole diagrams but also the coupling of Z^* to singly charged Higgs boson depends on c_{β^\pm} . This explains the bigger deviation of the fermion FB asymmetries in THM in comparison with other models. These effects could be tested at future colliders.

5. Conclusions

In this work, we have studied systematically one-loop corrections to the decay channels of the SM-like Higgs boson $h \rightarrow l\bar{l}\gamma$ with $l = \nu_{e,\mu,\tau}, e, \mu$, performed in three HESM frameworks, handling the computations in the HF gauge. The final formulas of one-loop form factors are expressed in terms of the logarithm and di-logarithmic functions, which have a great advantage for numerical investigation using simple numerical packages. In addition, we indicated that these analytic formulas can be reduced to the previous results of one-loop contributions to the decay channels $h \rightarrow \gamma\gamma, Z\gamma$, therefore confirming the consistency between them. Our results were used to investigate the enhancement factors of the decays $h \rightarrow l\bar{l}\gamma$ and the respective fermion FB asymmetries in the three particular HESM, namely the IDM, THDM, and THM. The numerical results show that R_{IDM} can approach the largest deviation of 10% from the SM prediction. On the other hand, both R_{THDM} and R_{THM} can reach larger deviation values of 30%. Last but not least, the IDM predicts values of the fermion FB asymmetries to be nearly the same as the SM value. In contrast, the two THDM and THM predict larger deviations from the SM, namely they can reach 30% and 50%, respectively. In conclusion, we have shown that direct impacts of mixing of neutral Higgs bosons and indirect effects of singly and doubly charged Higgs bosons exchanges to the decay channels $h \rightarrow l\bar{l}\gamma$ could be probed at future colliders.

Acknowledgment: This research is funded by Vietnam National Foundation for Science and Technology Development (NAFOSTED) under the grant number 103.01-2019.346

Appendix A. The couplings

Inert Doublet Model

Deriving all couplings in Table 1 for IDM are presented in this Appendix. We first collect the terms which give the coupling of SM-like Higgs to singly charged Higgs as follows:

$$\mathcal{L}_{\text{IDM}} \supset \lambda_3 |\Phi_1|^2 |\Phi_2|^2 \supset \frac{1}{2} \lambda_3 v^2 AA + \frac{1}{2} \lambda_3 v^2 H^\mp H^\pm + \frac{1}{4} \lambda_3 v^2 HH + \lambda_3 v h H^\mp H^\pm. \quad (\text{A.1})$$

From the kinetic terms in the IDM Lagrangian, one can derive the couplings of SM-like Higgs to gauge bosons as:

$$\begin{aligned} \mathcal{L}_{\text{IDM}} &= (D_\mu \Phi_1)^\dagger (D^\mu \Phi_1) + (D_\mu \Phi_2)^\dagger (D^\mu \Phi_2) \\ &\supset \left[\partial_\mu H^\mp + \frac{i}{2} (g_Z c_{2W} Z_\mu + g_Z s_{2W} \gamma_\mu) H^\mp + \frac{i}{2} g_2 W_\mu^- (H + iA) \right] \times \\ &\quad \times \left[\partial^\mu H^\pm - \frac{i}{2} (g_Z c_{2W} Z^\mu + g_Z s_{2W} \gamma^\mu) H^\pm - \frac{i}{2} g_2 W^{+\mu} (H + iA) \right] \\ &= \frac{i g_Z c_{2W}}{2} Z^\mu (H^\mp \partial_\mu H^\pm - \partial_\mu H^\mp H^\pm) + \frac{i g_Z s_{2W}}{2} \gamma^\mu (H^\mp \partial_\mu H^\pm - \partial_\mu H^\mp H^\pm) \\ &= i \frac{M_Z c_{2W}}{v} Z^\mu (H^\mp \partial_\mu H^\pm - \partial_\mu H^\mp H^\pm) + i \frac{2 M_W s_W}{v} A^\mu (H^\mp \partial_\mu H^\pm - \partial_\mu H^\mp H^\pm). \end{aligned} \quad (\text{A.2})$$

Where A_μ is photon field.

Two Higgs Doublet Model

We next derive all couplings in Table 2 for THDM in this Appendix. We expand the kinetic terms of Higgs Lagrangian in THDM,

$$\begin{aligned} \mathcal{L}_{\text{THDM}} &= (D_\mu \Phi_1)^\dagger (D^\mu \Phi_1) + (D_\mu \Phi_2)^\dagger (D^\mu \Phi_2) \\ &\supset i \frac{M_Z c_{2W}}{v} Z^\mu (H^\mp \partial_\mu H^\pm - \partial_\mu H^\mp H^\pm) + i \frac{M_Z s_{2W}}{v} A^\mu (H^\mp \partial_\mu H^\pm - \partial_\mu H^\mp H^\pm) \\ &\quad + \frac{M_Z^2 s_{\beta-\alpha}}{v} h Z^\mu Z_\mu + \frac{2 M_W^2 s_{\beta-\alpha}}{v} h W^\mu W_\mu. \end{aligned} \quad (\text{A.3})$$

The Higgs potential gives us the coupling for $hH^\pm H^\mp$,

$$\begin{aligned} \mathcal{V}_{\text{THDM}} &= \frac{\lambda_1}{2} (\Phi_1^\dagger \Phi_1)^2 + \frac{\lambda_2}{2} (\Phi_2^\dagger \Phi_2)^2 + \lambda_3 (\Phi_1^\dagger \Phi_1) (\Phi_2^\dagger \Phi_2) + \lambda_4 (\Phi_1^\dagger \Phi_2) (\Phi_2^\dagger \Phi_1) \\ &\quad + \lambda_5 [(\Phi_1^\dagger \Phi_2) (\Phi_2^\dagger \Phi_1)] \\ &\supset \left[\lambda_1 v c_\beta c_\alpha s_\beta^2 + \lambda_2 v s_\beta s_\alpha c_\beta^2 + \lambda_3 v [s_\beta s_\beta^2 s_\alpha + c_\beta c_\beta^2 c_\alpha] \right. \\ &\quad \left. - (\lambda_4 + \lambda_5) v s_\beta c_\beta (s_\beta c_\alpha + c_\beta s_\alpha) \right] \times h H^\pm H^\mp \\ &= \frac{1}{v} \left[(2\mu^2 - 2M_{H^\pm}^2 - 2m_h^2) s_{\beta-\alpha} + 2(\mu^2 - m_h^2) \cot_{2\beta} c_{\beta-\alpha} \right] h H^\pm H^\mp. \end{aligned} \quad (\text{A.4})$$

The generalized Yukawa Lagrangian of THDM is

$$-\mathcal{L}_Y = -\bar{Q}_L \frac{M_u}{v_i} \tilde{\Phi}_i u_R - \bar{Q}'_L \frac{M_d}{v_j} \Phi_j d_R - \bar{L}_L \frac{M_l}{v_k} \Phi_k l_R + h.c. \quad (\text{A.5})$$

Specifically, we have four Yukawa Lagrangian types as follows:

- Type I:

$$\begin{aligned}
-\mathcal{L}_Y^I &= -\bar{Q}_L \frac{M_u}{v_2} \tilde{\Phi}_2 u_R - \bar{Q}'_L \frac{M_d}{v_2} \Phi_2 d_R - \bar{L}_L \frac{M_l}{v_2} \Phi_2 l_R + h.c \\
&\supset \frac{M_l}{\sqrt{2}v} \frac{s_\alpha}{s_\beta} H \bar{e}_i e_i + \frac{M_l}{\sqrt{2}v} \frac{c_\alpha}{s_\beta} h \bar{e}_i e_i + i \frac{M_l \cot \beta \gamma^5}{\sqrt{2}v} A \bar{e}^i e^i \\
&\quad + \frac{M_u}{\sqrt{2}v} \frac{s_\alpha}{s_\beta} H \bar{u}^i u^i + \frac{M_u}{\sqrt{2}v} \frac{c_\alpha}{s_\beta} h \bar{u}^i u^i - i \frac{M_u \cot \beta \gamma^5}{\sqrt{2}v} A \bar{u}^i u^i \\
&\quad + \frac{M_d}{\sqrt{2}v} \frac{s_\alpha}{s_\beta} H \bar{d}^i d^i + \frac{M_d}{\sqrt{2}v} \frac{c_\alpha}{s_\beta} h \bar{d}^i d^i + i \frac{M_d \cot \beta \gamma^5}{\sqrt{2}v} A \bar{d}^i d^i.
\end{aligned} \tag{A.6}$$

- Type II:

$$\begin{aligned}
-\mathcal{L}_Y^{II} &= -\bar{Q}_L \frac{M_u}{v_2} \tilde{\Phi}_2 u_R - \bar{Q}'_L \frac{M_d}{v_1} \Phi_1 d_R - \bar{L}_L \frac{M_l}{v_1} \Phi_1 l_R + h.c \\
&\supset \frac{M_l}{\sqrt{2}v} \frac{c_\alpha}{c_\beta} H \bar{e}^i e^i - \frac{M_l}{\sqrt{2}v} \frac{s_\alpha}{c_\beta} h \bar{e}^i e^i - i \frac{M_l \gamma^5 \tan \beta}{\sqrt{2}v} A \bar{e}^i e^i \\
&\quad + \frac{M_d}{\sqrt{2}v} \frac{c_\alpha}{c_\beta} H \bar{d}^i d^i - \frac{M_d}{\sqrt{2}v} \frac{s_\alpha}{c_\beta} h \bar{d}^i d^i - i \frac{M_d \gamma^5 \tan \beta}{\sqrt{2}v} A \bar{d}^i d^i \\
&\quad + \frac{M_u}{\sqrt{2}v} \frac{s_\alpha}{s_\beta} H \bar{u}^i u^i + \frac{M_u}{\sqrt{2}v} \frac{c_\alpha}{s_\beta} h \bar{u}^i u^i - i \frac{M_u \gamma^5 \cot \beta}{\sqrt{2}v} A \bar{u}^i u^i.
\end{aligned} \tag{A.7}$$

- Type X:

$$\begin{aligned}
-\mathcal{L}_Y^X &= -\bar{Q}_L \frac{M_u}{v_2} \tilde{\Phi}_2 u_R - \bar{Q}'_L \frac{M_d}{v_2} \Phi_2 d_R - \bar{L}_L \frac{M_l}{v_1} \Phi_1 l_R + h.c \\
&\supset \frac{M_l}{\sqrt{2}v} \frac{c_\alpha}{c_\beta} H \bar{e}^i e^i - \frac{M_l}{\sqrt{2}v} \frac{s_\alpha}{c_\beta} h \bar{e}^i e^i - i \frac{M_l \gamma^5 \tan \beta}{\sqrt{2}v} A \bar{e}^i e^i \\
&\quad + \frac{M_d}{\sqrt{2}v} \frac{s_\alpha}{s_\beta} H \bar{d}^i d^i + \frac{M_d}{\sqrt{2}v} \frac{c_\alpha}{s_\beta} h \bar{d}^i d^i + i \frac{M_d \gamma^5 \cot \beta}{\sqrt{2}v} A \bar{d}^i d^i \\
&\quad + \frac{M_u}{\sqrt{2}v} \frac{s_\alpha}{s_\beta} H \bar{u}^i u^i + \frac{M_u}{\sqrt{2}v} \frac{c_\alpha}{s_\beta} h \bar{u}^i u^i - i \frac{M_u \gamma^5 \cot \beta}{\sqrt{2}v} A \bar{u}^i u^i.
\end{aligned} \tag{A.8}$$

- Type Y:

$$\begin{aligned}
-\mathcal{L}_Y^Y &= -\bar{Q}_L \frac{M_u}{v_2} \tilde{\Phi}_2 u_R - \bar{Q}'_L \frac{M_d}{v_1} \Phi_1 d_R - \bar{L}_L \frac{M_l}{v_2} \Phi_2 l_R + h.c \\
&\supset \frac{M_l}{\sqrt{2}v} \frac{s_\alpha}{s_\beta} H \bar{e}_i e_i + \frac{M_l}{\sqrt{2}v} \frac{c_\alpha}{s_\beta} h \bar{e}_i e_i + i \frac{M_l \gamma^5 \cot \beta}{\sqrt{2}v} A \bar{e}^i e^i \\
&\quad + \frac{M_u}{\sqrt{2}v} \frac{s_\alpha}{s_\beta} H \bar{u}^i u^i + \frac{M_u}{\sqrt{2}v} \frac{c_\alpha}{s_\beta} h \bar{u}^i u^i - i \frac{M_u \gamma^5 \cot \beta}{\sqrt{2}v} A \bar{u}^i u^i \\
&\quad + \frac{M_d}{\sqrt{2}v} \frac{c_\alpha}{c_\beta} H \bar{d}^i d^i - \frac{M_d}{\sqrt{2}v} \frac{s_\alpha}{c_\beta} h \bar{d}^i d^i - i \frac{M_d \gamma^5 \tan \beta}{\sqrt{2}v} A \bar{d}^i d^i.
\end{aligned} \tag{A.9}$$

Triplet Higgs Model

We expand the kinematic term in the Lagrangian of Triplet Higgs Model,

$$\begin{aligned}
\mathcal{L}_{\text{THM}} &= \text{Tr}[(D^\mu \Delta)^\dagger (D_\mu \Delta)] + (D^\mu \Phi)^\dagger (D_\mu \Phi) \\
&\supset ie A^\mu (H^\pm \partial_\mu H^\mp - H^\mp \partial_\mu H^\pm) \\
&+ i \frac{M_Z}{\sqrt{v^2 + 2v_\Delta^2}} (c_W^2 - s_W^2 - c_{\beta^\pm}^2) Z^\mu (H^\pm \partial_\mu H^\mp - H^\mp \partial_\mu H^\pm) \\
&+ \frac{2M_W^2}{v} (c_\alpha c_{\beta^\pm} + \sqrt{2} s_\alpha s_{\beta^\pm}) W^{\pm, \mu} W_\mu^\mp h + \frac{2M_Z^2}{\sqrt{v^2 + 2v_\Delta^2}} (c_{\beta^0} c_\alpha + 2s_{\beta^0} s_\alpha) Z^\mu Z_\mu h \\
&+ i \frac{2M_Z}{\sqrt{v^2 + 2v_\Delta^2}} (c_W^2 - s_W^2) Z^\mu (H^{\pm\pm} \partial_\mu H^{\mp\mp} - H^{\mp\mp} \partial_\mu H^{\pm\pm}) \\
&+ i(2e) A^\mu (H^{\pm\pm} \partial_\mu H^{\mp\mp} - H^{\mp\mp} \partial_\mu H^{\pm\pm}).
\end{aligned} \tag{A.10}$$

The Higgs potential gives us the couplings of $hH^{\pm\pm}H^{\mp\mp}$, $hH^\pm H^\mp$ as follows:

$$\begin{aligned}
\mathcal{V}_{\text{THM}} &= \frac{\lambda}{4} (\Phi^\dagger \Phi)^2 + \lambda_1 (\Phi^\dagger \Phi) \text{Tr}(\Delta^\dagger \Delta) + (\lambda_2 + \lambda_3) \text{Tr}(\Delta^\dagger \Delta)^2 + \lambda_4 \Phi^\dagger \Delta \Delta^\dagger \Phi \\
&\supset \left[\frac{\lambda}{2} s_{\beta^\pm}^2 v_\Phi c_\alpha + \lambda_1 (s_{\beta^\pm}^2 v_\Delta s_\alpha + c_{\beta^\pm}^2 v_\Phi c_\alpha) + 2(\lambda_2 + \lambda_3) c_{\beta^\pm}^2 v_\Delta s_\alpha \right. \\
&\quad \left. + \frac{\lambda_4}{2} (-\sqrt{2} s_{\beta^\pm} c_{\beta^\pm} (v_\Phi s_\alpha + v_\Delta c_\alpha) + v_\Phi c_\alpha c_{\beta^\pm}^2) \right] hH^\pm H^\mp \\
&+ \left[\lambda_1 v_\Phi c_\alpha + 2(\lambda_2 + \lambda_3) v_\Delta s_\alpha \right] hH^{\pm\pm} H^{\mp\mp}.
\end{aligned} \tag{A.11}$$

When $\frac{v_\Delta}{v_\Phi} \rightarrow 0$, one has $s_{\beta^\pm} \rightarrow 0$ and the resulting reads

$$g_{hH^\pm H^\mp}^{\text{THM}} = \lambda_1 v_\Phi c_\alpha + \frac{\lambda_4}{2} v_\Phi c_\alpha = \frac{v}{2} (2\lambda_1 + \lambda_4) c_\alpha = \lambda_1 v c_\alpha + \frac{2(M_{A^0}^2 - M_{H^\pm}^2)}{v} c_\alpha, \tag{A.12}$$

$$g_{hH^{\pm\pm} H^{\mp\mp}}^{\text{THM}} = \lambda_1 v_\Phi c_\alpha = \lambda_1 v c_\alpha. \tag{A.13}$$

Here $\lambda_1 \rightarrow \frac{4M_{H^\pm}^2 - 3M_{A^0}^2 + m_h^2}{v^2}$ and $2M_{H^\pm}^2 = M_{H^{\pm\pm}}^2 + M_{A^0}^2$. The Yukawa Lagrangian is to generate masses of neutrinos

$$\begin{aligned}
-\mathcal{L}_{\text{Yukawa}} &= -\mathcal{L}_{\text{Yukawa}}^{\text{SM}} + y_\nu l_L^T C(i\sigma_2 \Delta) l_L + \text{h.c} \\
&= y_\nu \begin{pmatrix} \nu_L^i & e_L^i \end{pmatrix} C \begin{pmatrix} 0 & 1 \\ -1 & 0 \end{pmatrix} \begin{pmatrix} \frac{\delta^\pm}{\sqrt{2}} & \delta^{\pm\pm} \\ \frac{1}{\sqrt{2}}(v_\Delta + \eta_\Delta + i\chi_\Delta) & -\frac{\delta^\pm}{\sqrt{2}} \end{pmatrix} \begin{pmatrix} \nu_L^i \\ e_L^i \end{pmatrix} + \text{h.c} \\
&= \frac{y_\nu v_\Delta}{\sqrt{2}} (\nu_L^i C \nu_L^i + \nu_L^i C^\dagger \nu_L^i) + \frac{y_\nu s_\alpha}{\sqrt{2}} h (\nu_L^i C \nu_L^i + \nu_L^i C^\dagger \nu_L^i) + \frac{y_\nu c_\alpha}{\sqrt{2}} H (\nu_L^i C \nu_L^i + \nu_L^i C^\dagger \nu_L^i) \\
&+ i \frac{y_\nu s_{\beta^0}}{\sqrt{2}} G^0 (\nu_L^i C \nu_L^i - \nu_L^i C^\dagger \nu_L^i) + i \frac{y_\nu c_{\beta^0}}{\sqrt{2}} A (\nu_L^i C \nu_L^i - \nu_L^i C^\dagger \nu_L^i) \\
&- \frac{y_\nu s_{\beta^\pm}}{\sqrt{2}} G^\pm (\nu_L^i C e_L^i + e_L^i C \nu_L^i) - \frac{y_\nu c_{\beta^\pm}}{\sqrt{2}} H^\pm (\nu_L^i C e_L^i + e_L^i C \nu_L^i) \\
&- \frac{y_\nu s_{\beta^\mp}}{\sqrt{2}} G^\mp (\nu_L^i C^\dagger e_L^i + e_L^i C^\dagger \nu_L^i) - \frac{y_\nu c_{\beta^\mp}}{\sqrt{2}} H^\mp (\nu_L^i C^\dagger e_L^i + e_L^i C^\dagger \nu_L^i) \\
&- y_\nu (\delta^{\pm\pm} e_L^i C e_L^i + \delta^{\mp\mp} e_L^i C^\dagger e_L^i).
\end{aligned} \tag{A.14}$$

Here we replace $\delta^{\pm\pm} = H^{\pm\pm}$ for later. We then collect all couplings related to the channels under consideration in THM as shown in Table 4.

Appendix B. Expressions for scalar one-loop integrals

Expressions for all scalar one-loop integrals in terms of logarithm and di-logarithm functions are presented in this appendix. The ϵ -expansions are performed with the help of `Package-X`. We have used the shorthand notation for kinematic variables as follows: $\tau_i = 4M_i^2/m_h^2$ and $\eta_i(\zeta_i) = 4M_i^2/q_{23}(q_{13})$, $\lambda_i = 4M_i^2/q_{12}$ where M_i can be one of masses $\{m_f, M_Z, M_W\}$. It is stress that internal masses are taken the form of $M_i^2 \rightarrow M_i^2 - i\rho$ for $\rho \rightarrow 0$ where Feynman's $i\rho$ prescription is taken into account. Expanding scalar one-loop integrals, there are exist the following parameters $1/\epsilon$ and μ^2 . The first parameter explains for UV -divergent part of Feynman loop integrals. The later parameter is to renormalization scale introducing to help to track of the correct dimension of the integrals in space-time dimension d . Besides that Spence functions $\text{Li}_2(x)$, ϵ -expansions for scalar box-integrals relate to Beenakker-Denner continued dilogarithm functions $\mathcal{L}i_2(x, y)$ as defined in [94].

- $\underline{B_0(m_h^2, M_i^2, M_i^2) - B_0(q_{23}, 0, M_i^2)}$:

Scalar one-loop two-point functions appear in our work can be expanded in terms of logarithm functions as follows:

$$B_0(m_h^2, M_i^2, M_i^2) = 2 + \frac{1}{\epsilon} - \log(M_i^2) + \sqrt{1 - \tau_i} \log \left[1 + \frac{2(\sqrt{1 - \tau_i} - 1)}{\tau_i} \right], \quad (\text{B.1})$$

$$B_0(q_{23}, 0, M_i^2) = 2 + \frac{1}{\epsilon} - \log(M_i^2) - \left(\frac{\eta_i}{4} - 1 \right) \log \left[\frac{\eta_i}{\eta_i - 4} \right]. \quad (\text{B.2})$$

Since internal masses takes $M_i^2 - i\rho$ for $\rho \rightarrow 0$, the logarithm functions in above are well defined in complex plane. Within the dimensional regularization, the ultraviolet divergences will be cancelled once subtract two scalar two-points integrals B_0 . In detail, we obtain the finite term as follows:

$$\begin{aligned} B_0(m_h^2, M_i^2, M_i^2) - B_0(q_{23}, 0, M_i^2) &= \\ &= \left(\frac{\eta_i}{4} - 1 \right) \log \left[\frac{\eta_i}{\eta_i - 4} \right] + \sqrt{1 - \tau_i} \log \left[1 + \frac{2(\sqrt{1 - \tau_i} - 1)}{\tau_i} \right]. \end{aligned} \quad (\text{B.3})$$

- $\underline{C_0(0, m_h^2, q_{23}(q_{13}), 0, M_i^2, M_i^2)}$:

Expansion for scalar one-loop three-point functions in this configuration is presented as

$$\begin{aligned} C_0(0, m_h^2, q_{23}, 0, M_i^2, M_i^2) &= \\ &= -\frac{\eta_i \tau_i}{4M_i^2(\eta_i - \tau_i)} \left\{ \text{Li}_2 \left[\frac{\eta_i}{\tau_i} + i\rho \frac{(\eta_i - 4)(\eta_i - \tau_i)}{\eta_i^3 \tau_i^2} \right] \right. \\ &\quad \left. + \text{Li}_2 \left[\frac{\eta_i(\tau_i - 4) + 4\tau_i}{\eta_i \tau_i + 2(\eta_i - \tau_i)(\sqrt{1 - \tau_i} - 1)} - i\rho \left\{ (\eta_i - \tau_i + 8)\eta_i^{-1} \tau_i^{-1} - 4(\eta_i^{-2} + \tau_i^{-2}) \right\} \right] \right. \\ &\quad \left. + \text{Li}_2 \left[\frac{\eta_i^2}{\eta_i^2 + 4(\tau_i - \eta_i)} + i\rho(4\eta_i^{-1} - 1) \right] - \text{Li}_2 \left[\frac{\eta_i^2(\tau_i - 4) + 4\eta_i \tau_i}{\tau_i(\eta_i^2 - 4\eta_i + 4\tau_i)} \right] \right. \\ &\quad \left. - \text{Li}_2 \left[\frac{\eta_i^2 - 4\eta_i + 4\tau_i}{\eta_i \tau_i} + i\rho \frac{(\eta_i - 4)(\eta_i - \tau_i)(\eta_i^2 - 4\eta_i + 4\tau_i)}{\eta_i^5 \tau_i^2} \right] \right\} \end{aligned} \quad (\text{B.4})$$

$$\begin{aligned}
& -\text{Li}_2 \left[\frac{\eta_i \tau_i}{\eta_i \tau_i + 2(\tau_i - \eta_i)(\sqrt{1 - \tau_i} + 1)} + i\rho(\tau_i^{-1} - \eta_i^{-1}) \right] \\
& + \text{Li}_2 \left[\frac{\eta_i(\tau_i - 4) + 4\tau_i}{\eta_i \tau_i + 2(\tau_i - \eta_i)(\sqrt{1 - \tau_i} + 1)} \right] - \text{Li}_2 \left[\frac{\eta_i \tau_i}{\eta_i \tau_i + 2(\eta_i - \tau_i)(\sqrt{1 - \tau_i} - 1)} \right] \Bigg\}.
\end{aligned}$$

Another C_0 function is obtained by

$$C_0(0, m_h^2, q_{13}, 0, M_i^2, M_i^2) = C_0(q_{13}, m_h^2, 0, 0, M_i^2, M_i^2). \quad (\text{B.5})$$

- $C_0(0, q_{12}, 0, 0, M_i^2, M_i^2)$:

For this kinematic configuration, C_0 function is expressed as:

$$\begin{aligned}
C_0(0, q_{12}, 0, 0, M_i^2, M_i^2) &= -\frac{\lambda_i}{24M_i^2} \left\{ \pi^2 - 6 \text{Li}_2 \left[\frac{\lambda_i}{\lambda_i + 2(\sqrt{1 - \lambda_i} - 1)} \right] \right. \\
&+ 6 \text{Li}_2 \left[\frac{\lambda_i - 4}{\lambda_i - 2(\sqrt{1 - \lambda_i} + 1)} \right] - 6 \text{Li}_2 \left[1 - \frac{4}{\lambda_i} \right] - 6 \text{Li}_2 \left[\frac{4 - \lambda_i}{2(\sqrt{1 - \lambda_i} + 1)} \right] \\
&\left. + 6 \text{Li}_2 \left[\frac{\lambda_i}{2(\sqrt{1 - \lambda_i} + 1)} \right] + 3 \log^2 \left[\frac{1}{2}(\sqrt{1 - \lambda_i} + 1) \right] - 3 \log^2 \left[\frac{\lambda_i + 2(\sqrt{1 - \lambda_i} - 1)}{2(\sqrt{1 - \lambda_i} + 1)} \right] \right\}. \quad (\text{B.6})
\end{aligned}$$

- $C_0(0, 0, q_{23}(q_{13}), 0, 0, M_i^2)$:

In further, one has

$$\begin{aligned}
C_0(0, 0, q_{23}, 0, 0, M_i^2) &= \\
&= \frac{\eta_i}{8M_i^2} \left\{ \log \left(\frac{\eta_i}{\eta_i - 4} \right) \left[\frac{2}{\epsilon} + \log \left(\frac{\eta_i}{\eta_i - 4} \right) + 2 \log \left(\frac{\mu^2}{M_i^2} \right) \right] - 2 \text{Li}_2 \left[\frac{4}{4 - \eta_i} \right] \right\}. \quad (\text{B.7})
\end{aligned}$$

- $C_0(0, 0, q_{23}(q_{13}), 0, M_i^2, M_i^2)$:

In additional, we have

$$C_0(0, 0, q_{23}, 0, M_i^2, M_i^2) = \frac{\eta_i}{8M_i^2} \left\{ 2 \text{Li}_2 \left[\frac{4}{4 - \eta_i} \right] + \log^2 \left[\frac{\eta_i}{\eta_i - 4} \right] \right\}. \quad (\text{B.8})$$

- $C_0(q_{12}, 0, m_h^2, M_i^2, M_i^2, M_i^2)$:

In this kinematic configuration, scalar one-loop three-point functions are expanded as

$$\begin{aligned}
C_0(q_{12}, 0, m_h^2, M_i^2, M_i^2, M_i^2) &= \\
&= \frac{\lambda_i \tau_i}{8M_i^2(\tau_i - \lambda_i)} \left\{ \log^2 \left[1 + \frac{2(\sqrt{1 - \lambda_i} - 1)}{\lambda_i} \right] - \log^2 \left[1 + \frac{2(\sqrt{1 - \tau_i} - 1)}{\tau_i} \right] \right\}. \quad (\text{B.9})
\end{aligned}$$

- $D_0(0, q_{13}, m_h^2, q_{23}, 0, 0, 0, 0, M_i^2, M_i^2)$:

Scalar one-loop box integrals for this kinematic configuration are derived as

$$D_0(0, q_{13}, m_h^2, q_{23}, 0, 0, 0, 0, M_i^2, M_i^2) =$$

$$\begin{aligned}
&= \frac{\eta_i \zeta_i}{8M_i^4(4 - \eta_i - \zeta_i)} \left\{ 2 \log \left(\frac{\eta_i}{\eta_i - 4} \right) \left[\frac{1}{\epsilon} + \log \left(\frac{\mu^2}{M_i^2} \right) + 2 \log \left(\frac{\zeta_i}{\zeta_i - 4} \right) \right] \right. \\
&\quad + \log \left(\frac{\zeta_i}{\zeta_i - 4} \right) \left[\frac{2}{\epsilon} + 2 \log \left(\frac{\mu^2}{M_i^2} \right) + \log \left(\frac{\zeta_i}{\zeta_i - 4} \right) \right] + \log^2 \left(\frac{\eta_i}{\eta_i - 4} \right) \\
&\quad + 2 \mathcal{L}i_2 \left[\frac{\eta_i - 4}{\eta_i} - i \frac{\rho}{\eta_i}, 1 - \frac{2(\sqrt{1 - \tau_i} + 1)}{\tau_i} - i \rho \frac{\sqrt{1 - \tau_i}}{\tau_i} \right] \\
&\quad + 2 \mathcal{L}i_2 \left[\frac{\eta_i - 4}{\eta_i} - i \frac{\rho}{\eta_i}, 1 + \frac{2(\sqrt{1 - \tau_i} - 1)}{\tau_i} + i \rho \times \frac{\sqrt{1 - \tau_i}}{\tau_i} \right] \\
&\quad + 4 \mathcal{L}i_2 \left[\frac{\eta_i}{\eta_i - 4} + i \frac{\rho}{\eta_i}, \frac{\zeta_i}{\zeta_i - 4} + i \frac{\rho}{\zeta_i} \right] - 4 \left[\text{Li}_2 \left(\frac{4}{4 - \eta_i} \right) + \text{Li}_2 \left(\frac{4}{4 - \zeta_i} \right) \right] \\
&\quad - 2 \mathcal{L}i_2 \left[1 - \frac{2(\sqrt{1 - \tau_i} + 1)}{\tau_i} - i \rho \frac{\sqrt{1 - \tau_i}}{\tau_i}, \frac{\zeta_i}{\zeta_i - 4} + i \frac{\rho}{\zeta_i} \right] \\
&\quad - 2 \mathcal{L}i_2 \left[1 + \frac{2(\sqrt{1 - \tau_i} - 1)}{\tau_i} + i \rho \frac{\sqrt{1 - \tau_i}}{\tau_i}, \frac{\zeta_i}{\zeta_i - 4} + i \frac{\rho}{\zeta_i} \right] \\
&\quad \left. + \left[\log \left(\frac{\eta_i}{\eta_i - 4} \right) + \log \left(\frac{\zeta_i}{\zeta_i - 4} \right) \right] \log \left[\frac{\eta_i(\zeta_i - 4)}{(\eta_i - 4)\zeta_i} + i \rho \left(\frac{\zeta_i - \eta_i}{\zeta_i \eta_i} \right) \right] \right\}. \tag{B.10}
\end{aligned}$$

- $D_0(0, q_{12}, 0, q_{23}(q_{13}), 0, m_h^2, 0, M_i^2, M_i^2, M_i^2)$:

Furthermore, we have another scalar box integrals for the following kinematic configuration which can be get the form of

$$\begin{aligned}
&D_0(0, q_{12}, 0, q_{23}, 0, m_h^2, 0, M_i^2, M_i^2, M_i^2) = \tag{B.11} \\
&= -\frac{\lambda_i \tau_i^{1/2}}{4M_i^4 \Delta(\tau_i, \lambda_i, \eta_i)} \left\{ \mathcal{L}i_2 \left[1 - 4\eta_i^{-1} - i \rho \times \eta_i^{-1}, \Delta^+(\tau_i, \lambda_i, \eta_i) + i \rho \times \Sigma(\tau_i, \lambda_i, \eta_i) \right] \right. \\
&\quad - \mathcal{L}i_2 \left[1 - 4\eta_i^{-1} - i \rho \times \eta_i^{-1}, \Delta^-(\tau_i, \lambda_i, \eta_i) - i \rho \times \Sigma(\tau_i, \lambda_i, \eta_i) \right] \\
&\quad + \mathcal{L}i_2 \left[\frac{\lambda_i}{\lambda_i - 2\Lambda^+} + i \rho \times \frac{[(\Lambda^+ + 1)\lambda_i - 2\Lambda^+]}{\lambda_i(\lambda_i - 2\Lambda^+)}, \Delta^+(\tau_i, \lambda_i, \eta_i) + i \rho \times \Sigma(\tau_i, \lambda_i, \eta_i) \right] \\
&\quad - \mathcal{L}i_2 \left[\frac{\lambda_i}{\lambda_i - 2\Lambda^+} + i \rho \times \frac{[(\Lambda^+ + 1)\lambda_i - 2\Lambda^+]}{\lambda_i(\lambda_i - 2\Lambda^+)}, \Delta^-(\tau_i, \lambda_i, \eta_i) - i \rho \times \Sigma(\tau_i, \lambda_i, \eta_i) \right] \\
&\quad + \mathcal{L}i_2 \left[\frac{\lambda_i}{\lambda_i + 2\Lambda^-} - i \rho \frac{[(\Lambda^- - 1) - 2\lambda_i^{-1}\Lambda^-]}{\lambda_i + 2\Lambda^-}, \Delta^+(\tau_i, \lambda_i, \eta_i) + i \rho \times \Sigma(\tau_i, \lambda_i, \eta_i) \right] \\
&\quad - \mathcal{L}i_2 \left[\frac{\lambda_i}{\lambda_i + 2\Lambda^-} - i \rho \frac{[(\Lambda^- - 1) - 2\lambda_i^{-1}\Lambda^-]}{\lambda_i + 2\Lambda^-}, \Delta^-(\tau_i, \lambda_i, \eta_i) - i \rho \times \Sigma(\tau_i, \lambda_i, \eta_i) \right] \\
&\quad - \mathcal{L}i_2 \left[1 - 4\tau_i^{-1} - i \rho \times \tau_i^{-1}, \Delta^+(\tau_i, \lambda_i, \eta_i) + i \rho \times \Sigma(\tau_i, \lambda_i, \eta_i) \right] \\
&\quad \left. + \mathcal{L}i_2 \left[1 - 4\tau_i^{-1} - i \rho \times \tau_i^{-1}, \Delta^-(\tau_i, \lambda_i, \eta_i) - i \rho \times \Sigma(\tau_i, \lambda_i, \eta_i) \right] \right\}
\end{aligned}$$

$$\begin{aligned}
& +\text{Li}_2 \left[\frac{\tau_i(\eta_i - 4) + \Delta(\tau_i, \lambda_i, \eta_i)\eta_i\sqrt{\tau_i}}{2\lambda_i(\eta_i - \tau_i)} + i\rho \times \Gamma^-(\tau_i, \lambda_i, \eta_i) \right] \\
& +\text{Li}_2 \left[\frac{\tau_i(\eta_i - 4) + \Delta(\tau_i, \lambda_i, \eta_i)\eta_i\sqrt{\tau_i}}{2\lambda_i(\eta_i - \tau_i)} + i\rho \times \Gamma^+(\tau_i, \lambda_i, \eta_i) \right] \\
& -\text{Li}_2 \left[\frac{\tau_i(\eta_i - 4) - \Delta(\tau_i, \lambda_i, \eta_i)\eta_i\sqrt{\tau_i}}{2\lambda_i(\eta_i - \tau_i)} + i\rho \times \Gamma^+(\tau_i, \lambda_i, \eta_i) \right] \\
& -\text{Li}_2 \left[\frac{\tau_i(\eta_i - 4) - \Delta(\tau_i, \lambda_i, \eta_i)\eta_i\sqrt{\tau_i}}{2\lambda_i(\eta_i - \tau_i)} + i\rho \times \Gamma^-(\tau_i, \lambda_i, \eta_i) \right] \Bigg\}.
\end{aligned}$$

Where related kinematic variables $\Delta^\pm, \Lambda^\pm, \Gamma^\pm, \Delta$ and Σ are defined in terms of dimensionless parameters $\tau_i, \lambda_i, \eta_i$ as follows:

$$\Delta(\tau_i, \lambda_i, \eta_i) = \left[\tau_i + 8\eta_i^{-2} \left(2\lambda_i\eta_i - 2\lambda_i\tau_i - \tau_i\eta_i + 2\tau_i \right) \right]^{1/2}, \quad (\text{B.12})$$

$$\Delta^\pm(\tau_i, \lambda_i, \eta_i) = \frac{2\tau_i(2 - \lambda_i) + \eta_i \left[2\lambda_i - \tau_i \pm \sqrt{\tau_i}\Delta(\tau_i, \lambda_i, \eta_i) \right]}{2\lambda_i(\eta_i - \tau_i)}, \quad (\text{B.13})$$

$$\Sigma(\tau_i, \lambda_i, \eta_i) = \frac{\lambda_i(\eta_i - \tau_i)}{M_i^2\eta_i\sqrt{\tau_i}\Delta(\tau_i, \lambda_i, \eta_i)}, \quad (\text{B.14})$$

$$\Lambda^\pm = \sqrt{1 - \lambda_i \pm 1} \quad (\text{B.15})$$

and

$$\begin{aligned}
\Gamma^\pm(\tau_i, \lambda_i, \eta_i) &= \frac{1}{2M_i^2\eta_i\lambda_i(\eta_i - \tau_i)\sqrt{\tau_i}\Delta(\tau_i, \lambda_i, \eta_i)} \times \quad (\text{B.16}) \\
&\times \left\{ -\eta_i^2 \left[2\lambda_i^2 \pm 2M_i^2\sqrt{\tau_i}\Delta(\tau_i, \lambda_i, \eta_i)\lambda_i \mp M_i^2\tau_i^{3/2} \left(\sqrt{\tau_i} + \Delta(\tau_i, \lambda_i, \eta_i) \right) \right] \right. \\
&+ 2\tau_i\eta_i \left[2\lambda_i^2 \pm M_i^2\lambda_i \left(\sqrt{\tau_i}\Delta(\tau_i, \lambda_i, \eta_i) + 8 \right) \mp 2M_i^2\sqrt{\tau_i} \left(2\sqrt{\tau_i} + \Delta(\tau_i, \lambda_i, \eta_i) \right) \right] \\
&\left. - 2\tau_i^2 \left[\lambda_i^2 \pm 8M_i^2(\lambda_i - 1) \right] \right\}.
\end{aligned}$$

Appendix C. Check for the calculations

We verify that the ultraviolet divergences for V^* -pole contributions come from the following term

$$B_0(m_h^2, M_i^2, M_i^2) - B_0(q_{23}, 0, M_i^2). \quad (\text{C.1})$$

This term gives a UV-finite result. In case of $F_{1,L}^{\text{Non-pole}, Z}$, we recognize that appearance of ultraviolet divergences by the ϵ^{-1} terms in such Passarino-Veltman functions

$$C_0(0, q_{13}(q_{23}), 0, 0, 0, M_Z^2) \text{ and } D_0(0, q_{13}, m_h^2, q_{23}, 0, 0, 0, 0, M_Z^2, M_Z^2)$$

as presented in next subsections. Therefore, we consider ϵ^{-1} terms and proof that divergences in the form factor are analytically eliminated as follows

$$\begin{aligned}
F_{1,L,UV\text{-term}}^{\text{Non-pole, Z}} &\supset q_{23}C_0(0, 0, q_{23}, 0, 0, M_Z^2) + q_{13}C_0(0, q_{13}, 0, 0, 0, M_Z^2) \\
&+ \left[M_Z^2(q_{13} + q_{23}) - q_{13}q_{23} \right] D_0(0, q_{13}, m_h^2, q_{23}, 0, 0, 0, 0, M_Z^2, M_Z^2) \\
&= \frac{4M_Z^2}{\eta_Z}C_0(0, 0, q_{23}, 0, 0, M_Z^2) + \frac{4M_Z^2}{\zeta_Z}C_0(0, q_{13}, 0, 0, 0, M_Z^2) \\
&+ 4M_Z^4 \left[\frac{\eta_Z + \zeta_Z - 4}{\eta_Z\zeta_Z} \right] D_0(0, q_{13}, m_h^2, q_{23}, 0, 0, 0, 0, M_Z^2, M_Z^2).
\end{aligned} \tag{C.2}$$

Kinematic variables η_Z and ζ_Z are defined as previous section. Expanding one-loop scalar integrals in terms of logarithm and di-logarithm functions, one has

$$\begin{aligned}
F_{1,L,UV\text{-term}}^{\text{Non-pole, Z}} &\supset \frac{4M_Z^2}{\eta_Z} \left[\frac{\eta_Z}{8M_Z^2} \log\left(\frac{\eta_Z}{\eta_Z - 4}\right) \right] \left[\frac{2}{\epsilon} + 2 \log\left(\frac{\mu^2}{M_Z^2}\right) \right] \\
&+ \frac{4M_Z^2}{\zeta_Z} \left[\frac{\zeta_Z}{8M_Z^2} \log\left(\frac{\zeta_Z}{\zeta_Z - 4}\right) \right] \left[\frac{2}{\epsilon} + 2 \log\left(\frac{\mu^2}{M_Z^2}\right) \right] \\
&+ 4M_Z^4 \left[\frac{\eta_Z + \zeta_Z - 4}{\eta_Z\zeta_Z} \right] \times \\
&\quad \times \left\{ \frac{\eta_Z\zeta_Z}{8M_Z^4(4 - \eta_Z - \zeta_Z)} \left[2 \log\left(\frac{\eta_Z}{\eta_Z - 4}\right) \left(\frac{1}{\epsilon} + \log\left(\frac{\mu^2}{M_Z^2}\right) \right) \right. \right. \\
&\quad \left. \left. + \log\left(\frac{\zeta_Z}{\zeta_Z - 4}\right) \left(\frac{2}{\epsilon} + 2 \log\left(\frac{\mu^2}{M_Z^2}\right) \right) \right] \right\} \\
&= \log\left(\frac{\eta_Z}{\eta_Z - 4}\right) \left[\frac{1}{\epsilon} + \log\left(\frac{\mu^2}{M_Z^2}\right) \right] + \log\left(\frac{\zeta_Z}{\zeta_Z - 4}\right) \left[\frac{1}{\epsilon} + \log\left(\frac{\mu^2}{M_Z^2}\right) \right] \\
&\quad - \frac{1}{2} \left\{ 2 \log\left(\frac{\eta_Z}{\eta_Z - 4}\right) \left[\frac{1}{\epsilon} + \log\left(\frac{\mu^2}{M_Z^2}\right) \right] \right. \\
&\quad \left. + \log\left(\frac{\zeta_Z}{\zeta_Z - 4}\right) \left[\frac{2}{\epsilon} + 2 \log\left(\frac{\mu^2}{M_Z^2}\right) \right] \right\} \\
&= 0.
\end{aligned}$$

The final results are independent of μ^2 and $1/\epsilon$.

Appendix D. The basic integrals I_1, I_2

The basic integrals I_1 and I_2 are taken in [93] and presented in term of f, g functions as follows:

$$I_1(\tau, \lambda) = \frac{\tau\lambda}{2(\tau - \lambda)} + \frac{\tau^2\lambda^2}{2(\tau - \lambda)^2} [f(\tau) - f(\lambda)] + \frac{\tau^2\lambda}{(\tau - \lambda)^2} [g(\tau) - g(\lambda)], \tag{D.1}$$

$$I_2(\tau, \lambda) = -\frac{\tau\lambda}{2(\tau - \lambda)} [f(\tau) - f(\lambda)]. \tag{D.2}$$

Two complex functions f , g can be expressed as follows:

$$f(\tau) = \begin{cases} \arcsin^2 \sqrt{\tau} & \text{for } \tau \leq 1, \\ -\frac{1}{4} \left[\log \frac{1 + \sqrt{1 - \tau^{-1}}}{1 - \sqrt{1 - \tau^{-1}}} - i\pi \right]^2 & \text{for } \tau > 1, \end{cases} \quad (\text{D.3})$$

and

$$g(\tau) = \begin{cases} \sqrt{\tau^{-1} - 1} \arcsin \sqrt{\tau} & \text{for } \tau \geq 1, \\ \frac{\sqrt{1 - \tau^{-1}}}{2} \left[\log \frac{1 + \sqrt{1 - \tau^{-1}}}{1 - \sqrt{1 - \tau^{-1}}} - i\pi \right] & \text{for } \tau < 1. \end{cases} \quad (\text{D.4})$$

Appendix E. Appendix E: Phase-space $1 \rightarrow 3$

In order to generate the forward-backward asymmetries, we are working on rest frame of Higgs boson. In this frame, involved kinematic variables are taken

$$\begin{aligned} q_{12} &= m_h^2 - 2m_h E_\gamma, \\ q_{13} &= m_l^2 + 2E_\gamma (E_1 - |\vec{p}_1| \cos \theta_l). \end{aligned} \quad (\text{E.1})$$

Where E_1 is energy of lepton and three momentum of lepton is taken as $|\vec{p}_1| = \sqrt{E_1^2 - m_l^2}$. The energy E_1 is then calculated as follows:

$$E_1 = \frac{\frac{m_h(m_h - E_\gamma)(m_h - 2E_\gamma)}{2} + \frac{E_\gamma \cos \theta_l}{2} \sqrt{m_h^2(m_h - 2E_\gamma)^2 + 4m_l^2 [E_\gamma^2 \cos^2 \theta_l - (E_\gamma - m_h)^2]}}{(E_\gamma - m_h)^2 - E_\gamma^2 \cos^2 \theta_l}. \quad (\text{E.2})$$

As a result, we present the differential decay rate with respect to E_γ and $\cos \theta$ as follows

$$\frac{d\Gamma}{dq_{12}q_{13}} = \frac{d\Gamma}{dE_\gamma \cos \theta_l} \times \left| \frac{\partial q_{12}}{\partial E_\gamma} \frac{\partial q_{13}}{\partial \cos \theta_l} - \frac{\partial q_{12}}{\partial \cos \theta_l} \frac{\partial q_{13}}{\partial E_\gamma} \right|^{-1}. \quad (\text{E.3})$$

We then perform the above integrand over $E_\gamma^{\text{cut}} \leq E_\gamma \leq \frac{m_h}{2}$ and $-1 \leq \cos \theta_l \leq +1$ or

$$\Gamma = \int_{E_\gamma^{\text{cut}}}^{\frac{m_h}{2}} dE_\gamma \int_{-1}^1 d \cos \theta_l \frac{d\Gamma}{dE_\gamma \cos \theta_l} \times \left| \frac{\partial q_{12}}{\partial E_\gamma} \frac{\partial q_{13}}{\partial \cos \theta_l} - \frac{\partial q_{12}}{\partial \cos \theta_l} \frac{\partial q_{13}}{\partial E_\gamma} \right|^{-1}. \quad (\text{E.4})$$

References

- [1] A. Liss *et al.* [ATLAS], [[arXiv:1307.7292](#) [hep-ex]].
- [2] [CMS], [[arXiv:1307.7135](#) [hep-ex]].
- [3] H. Baer, T. Barklow, K. Fujii, Y. Gao, A. Hoang, S. Kanemura, J. List, H. E. Logan, A. Nomerotski and M. Perelstein, *et al.* [[arXiv:1306.6352](#) [hep-ph]].

- [4] V. Khachatryan *et al.* [CMS], Eur. Phys. J. C **75** (2015) no.5, 212 doi:10.1140/epjc/s10052-015-3351-7 [[arXiv:1412.8662](#) [hep-ex]].
- [5] G. Aad *et al.* [ATLAS], Eur. Phys. J. C **76** (2016) no.1, 6 doi:10.1140/epjc/s10052-015-3769-y [[arXiv:1507.04548](#) [hep-ex]].
- [6] V. M. Abazov *et al.* [D0], Phys. Lett. B **671** (2009), 349-355 doi:10.1016/j.physletb.2008.12.009 [[arXiv:0806.0611](#) [hep-ex]].
- [7] S. Chatrchyan *et al.* [CMS], Phys. Lett. B **726** (2013), 587-609 doi:10.1016/j.physletb.2013.09.057 [[arXiv:1307.5515](#) [hep-ex]].
- [8] M. Aaboud *et al.* [ATLAS], JHEP **10** (2017), 112 doi:10.1007/JHEP10(2017)112 [[arXiv:1708.00212](#) [hep-ex]].
- [9] G. Aad *et al.* [ATLAS], Phys. Lett. B **809** (2020), 135754 doi:10.1016/j.physletb.2020.135754 [[arXiv:2005.05382](#) [hep-ex]].
- [10] V. Khachatryan *et al.* [CMS], Phys. Lett. B **753** (2016), 341-362 doi:10.1016/j.physletb.2015.12.039 [[arXiv:1507.03031](#) [hep-ex]].
- [11] A. M. Sirunyan *et al.* [CMS], JHEP **09** (2018), 148 doi:10.1007/JHEP09(2018)148 [[arXiv:1712.03143](#) [hep-ex]].
- [12] A. M. Sirunyan *et al.* [CMS], JHEP **11** (2018), 152 doi:10.1007/JHEP11(2018)152 [[arXiv:1806.05996](#) [hep-ex]].
- [13] G. Aad *et al.* [ATLAS], Phys. Lett. B **819** (2021), 136412 doi:10.1016/j.physletb.2021.136412 [[arXiv:2103.10322](#) [hep-ex]].
- [14] L. B. Chen, C. F. Qiao and R. L. Zhu, Phys. Lett. B **726** (2013), 306-311 [erratum: Phys. Lett. B **808** (2020), 135629] doi:10.1016/j.physletb.2013.08.050 [[arXiv:1211.6058](#) [hep-ph]].
- [15] J. S. Gainer, W. Y. Keung, I. Low and P. Schwaller, Phys. Rev. D **86** (2012), 033010 doi:10.1103/PhysRevD.86.033010 [[arXiv:1112.1405](#) [hep-ph]].
- [16] A. Y. Korchin and V. A. Kovalchuk, Eur. Phys. J. C **74** (2014) no.11, 3141 doi:10.1140/epjc/s10052-014-3141-7 [[arXiv:1408.0342](#) [hep-ph]].
- [17] A. Abbasabadi, D. Bowser-Chao, D. A. Dicus and W. W. Repko, Phys. Rev. D **52** (1995), 3919-3928.
- [18] A. Djouadi, V. Driesen, W. Hollik and J. Rosiek, Nucl. Phys. B **491** (1997), 68-102 doi:10.1016/S0550-3213(96)00711-0 [[arXiv:hep-ph/9609420](#) [hep-ph]].
- [19] A. Abbasabadi and W. W. Repko, Phys. Rev. D **62** (2000), 054025 doi:10.1103/PhysRevD.62.054025 [[arXiv:hep-ph/0004167](#) [hep-ph]].
- [20] D. A. Dicus and W. W. Repko, Phys. Rev. D **87** (2013) no.7, 077301 doi:10.1103/PhysRevD.87.077301 [[arXiv:1302.2159](#) [hep-ph]].
- [21] Y. Sun, H. R. Chang and D. N. Gao, JHEP **05** (2013), 061 doi:10.1007/JHEP05(2013)061 [[arXiv:1303.2230](#) [hep-ph]].

- [22] G. Passarino, Phys. Lett. B **727** (2013), 424-431 doi:10.1016/j.physletb.2013.10.052 [[arXiv:1308.0422](#) [hep-ph]].
- [23] D. A. Dicus, C. Kao and W. W. Repko, Phys. Rev. D **89** (2014) no.3, 033013 doi:10.1103/PhysRevD.89.033013 [[arXiv:1310.4380](#) [hep-ph]].
- [24] A. Kachanovich, U. Nierste and I. Nišandžić, Phys. Rev. D **101** (2020) no.7, 073003 doi:10.1103/PhysRevD.101.073003 [[arXiv:2001.06516](#) [hep-ph]].
- [25] C. S. Li, C. F. Qiao and S. H. Zhu, Phys. Rev. D **57** (1998), 6928-6933 doi:10.1103/PhysRevD.57.6928 [[arXiv:hep-ph/9801334](#) [hep-ph]].
- [26] K. Sasaki and T. Uematsu, Phys. Lett. B **781** (2018), 290-294 doi:10.1016/j.physletb.2018.04.005 [[arXiv:1712.00197](#) [hep-ph]].
- [27] K. H. Phan, L. Hue and D. T. Tran, PTEP **2021** (2021) no.10, 103B07 doi:10.1093/ptep/ptab121 [[arXiv:2106.14466](#) [hep-ph]].
- [28] V. Van On, D. T. Tran, C. L. Nguyen and K. H. Phan, Eur. Phys. J. C **82** (2022) no.3, 277 doi:10.1140/epjc/s10052-022-10225-z [[arXiv:2111.07708](#) [hep-ph]].
- [29] W. J. Marciano, C. Zhang and S. Willenbrock, Phys. Rev. D **85** (2012), 013002 doi:10.1103/PhysRevD.85.013002 [[arXiv:1109.5304](#) [hep-ph]].
- [30] A. Djouadi, V. Driesen, W. Hollik and A. Kraft, Eur. Phys. J. C **1** (1998), 163-175 doi:10.1007/BF01245806 [[arXiv:hep-ph/9701342](#) [hep-ph]].
- [31] L. T. Hue, A. B. Arbuzov, T. T. Hong, T. P. Nguyen, D. T. Si and H. N. Long, Eur. Phys. J. C **78** (2018) no.11, 885 doi:10.1140/epjc/s10052-018-6349-0 [[arXiv:1712.05234](#) [hep-ph]].
- [32] K. H. Phan and D. T. Tran, PTEP **2020** (2020) no.5, 053B08 doi:10.1093/ptep/ptaa061 [[arXiv:2004.03213](#) [hep-ph]].
- [33] K. H. Phan, L. Hue and D. T. Tran, PTEP **2021** (2021) no.9, 093B05 doi:10.1093/ptep/ptab106 [[arXiv:2103.14248](#) [hep-ph]].
- [34] J. C. Pati and A. Salam, Phys. Rev. D **10**, 275-289 (1974) [erratum: Phys. Rev. D **11**, 703-703 (1975)].
- [35] R. N. Mohapatra and J. C. Pati, Phys. Rev. D **11**, 2558 (1975).
- [36] G. Senjanovic and R. N. Mohapatra, Phys. Rev. D **12**, 1502 (1975).
- [37] M. Singer, J. W. F. Valle and J. Schechter, Phys. Rev. D **22**, 738 (1980).
- [38] J. W. F. Valle and M. Singer, Phys. Rev. D **28**, 540 (1983).
- [39] F. Pisano and V. Pleitez, Phys. Rev. D **46**, 410-417 (1992).
- [40] P. H. Frampton, Phys. Rev. Lett. **69**, 2889-2891 (1992).
- [41] R. A. Diaz, R. Martinez and F. Ochoa, Phys. Rev. D **72**, 035018 (2005).
- [42] R. M. Fonseca and M. Hirsch, JHEP **08** (2016), 003

- [43] R. Foot, H. N. Long and T. A. Tran, Phys. Rev. D **50**, no.1, R34-R38 (1994).
- [44] L. A. Sanchez, F. A. Perez and W. A. Ponce, Eur. Phys. J. C **35** (2004), 259-265 [[arXiv:hep-ph/0404005](#) [hep-ph]].
- [45] W. A. Ponce and L. A. Sanchez, Mod. Phys. Lett. A **22** (2007), 435-448 [[arXiv:hep-ph/0607175](#) [hep-ph]].
- [46] Riazuddin and Fayyazuddin, Eur. Phys. J. C **56** (2008), 389-394 [[arXiv:0803.4267](#) [hep-ph]].
- [47] A. Jaramillo and L. A. Sanchez, Phys. Rev. D **84** (2011), 115001 [[arXiv:1110.3363](#) [hep-ph]].
- [48] H. N. Long, L. T. Hue and D. V. Loi, Phys. Rev. D **94** (2016) no.1, 015007 [[arXiv:1605.07835](#) [hep-ph]].
- [49] D. Borah and J. M. Cline, Phys. Rev. D **86** (2012), 055001 doi:10.1103/PhysRevD.86.055001 [[arXiv:1204.4722](#) [hep-ph]].
- [50] M. Gustafsson, S. Rydbeck, L. Lopez-Honorez and E. Lundstrom, Phys. Rev. D **86** (2012), 075019 doi:10.1103/PhysRevD.86.075019 [[arXiv:1206.6316](#) [hep-ph]].
- [51] A. Arhrib, R. Benbrik and N. Gaur, Phys. Rev. D **85** (2012), 095021 doi:10.1103/PhysRevD.85.095021 [[arXiv:1201.2644](#) [hep-ph]].
- [52] M. Klasen, C. E. Yaguna and J. D. Ruiz-Alvarez, Phys. Rev. D **87** (2013), 075025 doi:10.1103/PhysRevD.87.075025 [[arXiv:1302.1657](#) [hep-ph]].
- [53] M. Krawczyk, D. Sokolowska, P. Swaczyna and B. Swiezewska, JHEP **09** (2013), 055 doi:10.1007/JHEP09(2013)055 [[arXiv:1305.6266](#) [hep-ph]].
- [54] A. Arhrib, R. Benbrik and T. C. Yuan, Eur. Phys. J. C **74** (2014), 2892 doi:10.1140/epjc/s10052-014-2892-5 [[arXiv:1401.6698](#) [hep-ph]].
- [55] N. Chakrabarty, D. K. Ghosh, B. Mukhopadhyaya and I. Saha, Phys. Rev. D **92** (2015) no.1, 015002 doi:10.1103/PhysRevD.92.015002 [[arXiv:1501.03700](#) [hep-ph]].
- [56] A. Ilnicka, M. Krawczyk and T. Robens, Phys. Rev. D **93** (2016) no.5, 055026 doi:10.1103/PhysRevD.93.055026 [[arXiv:1508.01671](#) [hep-ph]].
- [57] A. Datta, N. Ganguly, N. Khan and S. Rakshit, Phys. Rev. D **95** (2017) no.1, 015017 doi:10.1103/PhysRevD.95.015017 [[arXiv:1610.00648](#) [hep-ph]].
- [58] J. Kalinowski, W. Kotlarski, T. Robens, D. Sokolowska and A. F. Zarnecki, JHEP **12** (2018), 081 doi:10.1007/JHEP12(2018)081 [[arXiv:1809.07712](#) [hep-ph]].
- [59] D. Dercks and T. Robens, Eur. Phys. J. C **79** (2019) no.11, 924 doi:10.1140/epjc/s10052-019-7436-6 [[arXiv:1812.07913](#) [hep-ph]].
- [60] C. W. Chiang and K. Yagyu, Phys. Rev. D **87** (2013) no.3, 033003 doi:10.1103/PhysRevD.87.033003 [[arXiv:1207.1065](#) [hep-ph]].
- [61] R. Benbrik, M. Boukidi, M. Ouchemhou, L. Rahili and O. Tibsirte, Nucl. Phys. B **990** (2023), 116154 doi:10.1016/j.nuclphysb.2023.116154 [[arXiv:2211.12546](#) [hep-ph]].

- [62] G. C. Branco, P. M. Ferreira, L. Lavoura, M. N. Rebelo, M. Sher and J. P. Silva, Phys. Rept. **516** (2012), 1-102 doi:10.1016/j.physrep.2012.02.002 [[arXiv:1106.0034](#) [hep-ph]].
- [63] S. Nie and M. Sher, Phys. Lett. B **449** (1999), 89-92 doi:10.1016/S0370-2693(99)00019-2 [[arXiv:hep-ph/9811234](#) [hep-ph]].
- [64] S. Kanemura, T. Kasai and Y. Okada, Phys. Lett. B **471** (1999), 182-190 doi:10.1016/S0370-2693(99)01351-9 [[arXiv:hep-ph/9903289](#) [hep-ph]].
- [65] A. G. Akeroyd, A. Arhrib and E. M. Naimi, Phys. Lett. B **490** (2000), 119-124 doi:10.1016/S0370-2693(00)00962-X [[arXiv:hep-ph/0006035](#) [hep-ph]].
- [66] I. F. Ginzburg and I. P. Ivanov, Phys. Rev. D **72** (2005), 115010 doi:10.1103/PhysRevD.72.115010 [[arXiv:hep-ph/0508020](#) [hep-ph]].
- [67] S. Kanemura, Y. Okada, H. Taniguchi and K. Tsumura, Phys. Lett. B **704** (2011), 303-307 doi:10.1016/j.physletb.2011.09.035 [[arXiv:1108.3297](#) [hep-ph]].
- [68] S. Kanemura and K. Yagyu, Phys. Lett. B **751** (2015), 289-296 doi:10.1016/j.physletb.2015.10.047 [[arXiv:1509.06060](#) [hep-ph]].
- [69] L. Bian and N. Chen, JHEP **09** (2016), 069 doi:10.1007/JHEP09(2016)069 [[arXiv:1607.02703](#) [hep-ph]].
- [70] W. Xie, R. Benbrik, A. Habjia, S. Taj, B. Gong and Q. S. Yan, Phys. Rev. D **103** (2021) no.9, 095030 doi:10.1103/PhysRevD.103.095030 [[arXiv:1812.02597](#) [hep-ph]].
- [71] E. J. Chun, H. M. Lee and P. Sharma, JHEP **11** (2012), 106 doi:10.1007/JHEP11(2012)106 [[arXiv:1209.1303](#) [hep-ph]].
- [72] C. S. Chen, C. Q. Geng, D. Huang and L. H. Tsai, Phys. Lett. B **723** (2013), 156-160 doi:10.1016/j.physletb.2013.05.007 [[arXiv:1302.0502](#) [hep-ph]].
- [73] A. Arhrib, R. Benbrik, M. Chabab, G. Moultaqa, M. C. Peyranere, L. Rahili and J. Ramadan, Phys. Rev. D **84** (2011), 095005 doi:10.1103/PhysRevD.84.095005 [[arXiv:1105.1925](#) [hep-ph]].
- [74] A. Arhrib, R. Benbrik, M. Chabab, G. Moultaqa and L. Rahili, JHEP **04** (2012), 136 doi:10.1007/JHEP04(2012)136 [[arXiv:1112.5453](#) [hep-ph]].
- [75] A. G. Akeroyd and S. Moretti, Phys. Rev. D **86** (2012), 035015 doi:10.1103/PhysRevD.86.035015 [[arXiv:1206.0535](#) [hep-ph]].
- [76] A. G. Akeroyd and H. Sugiyama, Phys. Rev. D **84** (2011), 035010 doi:10.1103/PhysRevD.84.035010 [[arXiv:1105.2209](#) [hep-ph]].
- [77] A. G. Akeroyd and S. Moretti, Phys. Rev. D **84** (2011), 035028 doi:10.1103/PhysRevD.84.035028 [[arXiv:1106.3427](#) [hep-ph]].
- [78] M. Aoki, S. Kanemura and K. Yagyu, Phys. Rev. D **85** (2012), 055007 doi:10.1103/PhysRevD.85.055007 [[arXiv:1110.4625](#) [hep-ph]].
- [79] S. Kanemura and K. Yagyu, Phys. Rev. D **85** (2012), 115009 doi:10.1103/PhysRevD.85.115009 [[arXiv:1201.6287](#) [hep-ph]].

- [80] M. Chabab, M. C. Peyranere and L. Rahili, Phys. Rev. D **90** (2014) no.3, 035026 doi:10.1103/PhysRevD.90.035026 [[arXiv:1407.1797](#) [hep-ph]].
- [81] Z. L. Han, R. Ding and Y. Liao, Phys. Rev. D **91** (2015), 093006 doi:10.1103/PhysRevD.91.093006 [[arXiv:1502.05242](#) [hep-ph]].
- [82] M. Chabab, M. C. Peyranère and L. Rahili, Phys. Rev. D **93** (2016) no.11, 115021 doi:10.1103/PhysRevD.93.115021 [[arXiv:1512.07280](#) [hep-ph]].
- [83] N. Haba, H. Ishida, N. Okada and Y. Yamaguchi, Eur. Phys. J. C **76** (2016) no.6, 333 doi:10.1140/epjc/s10052-016-4180-z [[arXiv:1601.05217](#) [hep-ph]].
- [84] D. K. Ghosh, N. Ghosh, I. Saha and A. Shaw, Phys. Rev. D **97** (2018) no.11, 115022 doi:10.1103/PhysRevD.97.115022 [[arXiv:1711.06062](#) [hep-ph]].
- [85] S. Ashanujjaman and K. Ghosh, JHEP **03** (2022), 195 doi:10.1007/JHEP03(2022)195 [[arXiv:2108.10952](#) [hep-ph]].
- [86] R. Zhou, L. Bian and Y. Du, JHEP **08** (2022), 205 doi:10.1007/JHEP08(2022)205 [[arXiv:2203.01561](#) [hep-ph]].
- [87] M. Aoki, S. Kanemura, M. Kikuchi and K. Yagyu, Phys. Rev. D **87** (2013) no.1, 015012 doi:10.1103/PhysRevD.87.015012 [[arXiv:1211.6029](#) [hep-ph]].
- [88] T. Hahn, Comput. Phys. Commun. **140** (2001), 418-431 doi:10.1016/S0010-4655(01)00290-9 [[arXiv:hep-ph/0012260](#) [hep-ph]].
- [89] T. Hahn and M. Perez-Victoria, Comput. Phys. Commun. **118** (1999), 153-165.
- [90] R. Mertig, M. Bohm and A. Denner, Comput. Phys. Commun. **64** (1991), 345-359 doi:10.1016/0010-4655(91)90130-D
- [91] H. H. Patel, Comput. Phys. Commun. **197** (2015), 276-290
- [92] A. Denner and S. Dittmaier, Nucl. Phys. B **734** (2006), 62-115
- [93] A. Djouadi, Phys. Rept. **457** (2008), 1-216 doi:10.1016/j.physrep.2007.10.004 [[arXiv:hep-ph/0503172](#) [hep-ph]].
- [94] W. Beenakker and A. Denner, Nucl. Phys. B **338** (1990), 349-370 doi:10.1016/0550-3213(90)90636-R.

(M_{H^\pm}, μ_2) [GeV]	$(R_{\text{IDM}}^{(e)}, \mathcal{A}_{\text{FB}}^{(e)})$	$(R_{\text{IDM}}^{(\mu)}, \mathcal{A}_{\text{FB}}^{(\mu)})$
(200, ± 200)	(1.0109 , 0.3689)	(1.0126 , 0.2860)
(400, ± 100)	(0.9491 , 0.3617)	(0.9579 , 0.2758)
(400, ± 200)	(0.9592 , 0.3639)	(0.9662 , 0.2779)
(400, ± 400)	(1.0057 , 0.3690)	(1.0036 , 0.2859)
(800, ± 100)	(0.9472 , 0.3613)	(0.9564 , 0.2754)
(800, ± 200)	(0.9497 , 0.3618)	(0.9584 , 0.2759)
(800, ± 400)	(0.9696 , 0.3613)	(0.9666 , 0.2779)
(1000, ± 100)	(0.9470 , 0.3613)	(0.9562 , 0.2753)
(1000, ± 200)	(0.9485 , 0.3616)	(0.9575 , 0.2757)

Table 8: The enhancement factor $R_{\text{IDM}}^{(l)}$ and integrated FB asymmetries $\mathcal{A}_{\text{FB}}^{(l)}$ with $l = e, \mu$ in the IDM framework. The masses are in GeV. The SM values are $\mathcal{A}_{\text{FB}}^{(e)} = 0.3673$ and $\mathcal{A}_{\text{FB}}^{(\mu)} = 0.2843$.

$(t_\beta, s_{\beta-\alpha}, M_{H^\pm}, M_H)$	$(R_{\text{THDM}}^{(e)}, \mathcal{A}_{\text{FB}}^{(e)})$	$(R_{\text{THDM}}^{(\mu)}, \mathcal{A}_{\text{FB}}^{(\mu)})$
$(5, 0.95, 200, 400)$	$(0.9516, 0.3548)$ $(0.9424, 0.3543)$	$(0.8754, 0.3221)$ $(0.8135, 0.3415)$
$(5, 0.99, 400, 200)$	$(0.9946, 0.3487)$ $(0.9925, 0.3499)$	$(0.9119, 0.3176)$ $(0.8276, 0.3483)$
$(10, 0.95, 400, 600)$	$(0.8439, 0.3338)$ $(0.8423, 0.3431)$	$(0.7809, 0.3017)$ $(1.1276, 0.2448)$
$(10, 0.99, 600, 400)$	$(0.9968, 0.3493)$ $(0.9972, 0.3512)$	$(0.9112, 0.3190)$ $(0.8573, 0.3478)$
$(15, 0.95, 800, 600)$	$(0.8721, 0.3399)$ $(0.8875, 0.3469)$	$(0.8025, 0.3088)$ $(1.9386, 0.1499)$
$(15, 0.99, 600, 800)$	$(0.9851, 0.3473)$ $(0.9879, 0.3558)$	$(0.9007, 0.3172)$ $(0.9299, 0.3154)$
$(20, 0.95, 500, 1000)$	$(0.5310, 0.2421)$ $(0.5469, 0.2466)$	$(0.5197, 0.2097)$ $(2.8866, 0.0687)$
$(20, 0.99, 1000, 500)$	$(0.9857, 0.3474)$ $(0.9935, 0.3557)$	$(0.9008, 0.3174)$ $(1.1117, 0.2737)$

Table 9: The enhancement factor $R_{\text{THDM}}^{(l)}$ and integrated FB asymmetries $\mathcal{A}_{\text{FB}}^{(l)}$ with $l = e, \mu$ in the THDM types I (first line) and X (second line). The masses are shown in GeV.

$(t_\beta, s_{\beta-\alpha}, M_{H^\pm}, M_H)$	$(R_{\text{THDM}}^{(e)}, \mathcal{A}_{\text{FB}}^{(e)})$	$(R_{\text{THDM}}^{(\mu)}, \mathcal{A}_{\text{FB}}^{(\mu)})$
$(5, 0.95, 800, 600)$	$(0.9133, 0.3536)$ $(0.9150, 0.3577)$	$(0.7998, 0.3476)$ $(0.8569, 0.3296)$
$(5, 0.99, 600, 800)$	$(1.0573, 0.3634)$ $(1.0576, 0.3621)$	$(0.8899, 0.3598)$ $(0.9643, 0.3356)$
$(10, 0.95, 500, 1000)$	$(0.7885, 0.3215)$ $(0.7967, 0.3245)$	$(1.0588, 0.2123)$ $(0.7378, 0.2901)$
$(10, 0.99, 1000, 500)$	$(0.9903, 0.3532)$ $(0.9908, 0.3523)$	$(0.8389, 0.3478)$ $(0.9136, 0.3228)$
$(15, 0.95, 800, 600)$	$(0.8654, 0.3476)$ $(0.8675, 0.3429)$	$(1.9231, 0.1498)$ $(0.8091, 0.3477)$
$(15, 0.99, 600, 800)$	$(0.9867, 0.3567)$ $(0.9841, 0.3539)$	$(0.9273, 0.3132)$ $(0.9002, 0.3297)$
$(20, 0.95, 500, 1000)$	$(0.5455, 0.2521)$ $(0.5256, 0.2452)$	$(2.8719, 0.0732)$ $(0.5207, 0.2087)$
$(20, 0.99, 1000, 500)$	$(0.9849, 0.3537)$ $(0.9888, 0.3567)$	$(1.0996, 0.2667)$ $(0.9047, 0.3227)$

Table 10: The enhancement factor $R_{\text{THDM}}^{(l)}$ and integrated FB asymmetries $\mathcal{A}_{\text{FB}}^{(l)}$ with $l = e, \mu$ in the THDM types II (first line) and Type Y (second line data), respectively. The masses are presented in GeV.

$(M_{H^\pm}, M_{H^{\pm\pm}}, \lambda_1)$	$(R_{\text{THM}}^{(e)}, \mathcal{A}_{\text{FB}}^{(e)})$	$(R_{\text{THM}}^{(\mu)}, \mathcal{A}_{\text{FB}}^{(\mu)})$
$(100, 400, +4)$	$(0.7942, 0.3086)$ $(0.7475, 0.3152)$	$(0.8257, 0.2480)$ $(0.7769, 0.2532)$
$(200, 500, +4)$	$(0.8573, 0.2907)$ $(0.8104, 0.2955)$	$(0.8768, 0.2374)$ $(0.8278, 0.2414)$
$(400, 600, +4)$	$(0.8997, 0.2644)$ $(0.8514, 0.2672)$	$(0.9104, 0.2182)$ $(0.8611, 0.2208)$
$(600, 600, +4)$	$(0.9057, 0.2513)$ $(0.8584, 0.2532)$	$(0.9161, 0.2080)$ $(0.8667, 0.2099)$
$(1000, 1000, +4)$	$(0.9452, 0.2612)$ $(0.8981, 0.2637)$	$(0.9481, 0.2175)$ $(0.8989, 0.2199)$
$(150, 400, -4)$	$(1.1449, 0.5012)$ $(1.1106, 0.5166)$	$(1.1099, 0.4245)$ $(1.0712, 0.4395)$
$(200, 600, -4)$	$(1.0489, 0.4778)$ $(1.0013, 0.4930)$	$(1.0240, 0.3989)$ $(0.9826, 0.4130)$
$(400, 700, -4)$	$(1.0013, 0.3198)$ $(0.9558, 0.3260)$	$(0.9935, 0.2673)$ $(0.9457, 0.2732)$
$(800, 800, -4)$	$(1.0042, 0.2751)$ $(0.9577, 0.2784)$	$(0.9959, 0.2309)$ $(0.9473, 0.2342)$
$(1000, 400, -4)$	$(1.1414, 0.2773)$ $(1.0862, 0.2806)$	$(1.0990, 0.2369)$ $(1.0514, 0.2404)$

Table 11: The enhancement factor for the decay rates $R_{\text{THM}}^{(l)}$ and integrated FB asymmetries $\mathcal{A}_{\text{FB}}^{(l)}$ with $l = e, \mu$ in the THM. The first (second) line shows the numerical values of fixed $c_\alpha = 0.98, v_\Delta = 5$ MeV ($c_\alpha = 0.95, v_\Delta = 1$ MeV). The masses are shown in GeV.